

Electronic Thesis and Dissertation Repository

8-19-2022 10:00 AM

Thermo-responsive Antibiotic-Eluting Coatings for Treating Infection near Orthopedic Implants


Jan Chung Kwan, *The University of Western Ontario*

Supervisor: Gillies, Elizabeth, *The University of Western Ontario*

A thesis submitted in partial fulfillment of the requirements for the Master of Engineering Science degree in Biomedical Engineering

© Jan Chung Kwan 2022

Follow this and additional works at: <https://ir.lib.uwo.ca/etd>

 Part of the [Bacteria Commons](#), [Biomaterials Commons](#), [Other Chemicals and Drugs Commons](#), [Polymer and Organic Materials Commons](#), and the [Polymer Chemistry Commons](#)

Recommended Citation

Kwan, Jan Chung, "Thermo-responsive Antibiotic-Eluting Coatings for Treating Infection near Orthopedic Implants" (2022). *Electronic Thesis and Dissertation Repository*. 8816.
<https://ir.lib.uwo.ca/etd/8816>

This Dissertation/Thesis is brought to you for free and open access by Scholarship@Western. It has been accepted for inclusion in Electronic Thesis and Dissertation Repository by an authorized administrator of Scholarship@Western. For more information, please contact wlsadmin@uwo.ca.

Abstract

The clinical effectiveness of orthopedic devices to restore the function of joints has been well established yet there is a lack of development in associated infections. As the demand for orthopedic surgeries continues to rise, infection remains a growing problem and one of the main reasons for revision surgeries. Bacterial contamination of the surgical site followed by adhesion of bacteria onto the surface of orthopedic devices leads to the formation of a biofilm which is a common initiator for infection. As a result, infection in the orthopedic field is commonly defined as orthopedic device-related infections (ODRI). There are limited options to treat ODRI, with revision surgery being the most common standard of treatment involving multiple surgeries to replace the infected component, but this approach is very expensive and can reduce the quality of life for the patient. Although the use of antibiotic carriers such as poly(methyl methacrylate) (PMMA) bone cement and calcium sulfate have shown promise, their ability to control the amount and rate of drug release remains a challenge. In this study, I have investigated a novel approach in using induction heating (IH) to not only directly kill bacteria and inhibit biofilm formation but also achieve on-demand externally triggered release of antibiotics from a poly(ester amide) (PEA) coating. The PEA coating has a glass transition temperature (T_g) of 39 °C, just above physiological temperature. I demonstrated that by heating the PEA above its T_g , either by direct heating or IH, the release of antibiotics can be accelerated due to the increased mobility of the drug in the PEA film in its rubbery state. The use of an intermittent IH protocol paired with an antibiotic-loaded PEA coating leads to a synergistic reduction in biofilm formation and live bacteria on the surfaces of the coating. This new technology provides a promising new approach to potentially prevent and treat implant-associated orthopedic infections.

Keywords

Orthopedic device-related infection, antibiotic, bone and joint, local drug delivery, polymer coating, induction heating, biofilm, bacteria, implants.

Summary for Lay Audience

Orthopedic device-related infections (ODRI) have been a growing problem within the orthopedic field and are one of the major reasons for revision surgery. As the demand for hip and knee replacements continues to rise, infections near orthopedic devices will follow suit. Infections are often associated with bacteria that adhere to metallic surfaces. If left untreated, they can grow in size and complexity while acting as a protective environment for bacteria. Not only are these infections difficult to treat with antibiotics, but they can also lead to antibiotic-resistant bacteria if not properly treated. The most common treatment is a two-stage revision surgery involving multiple surgeries to replace the infected component while being administered oral or intravenous antibiotics. However, this approach is expensive and reduces the quality of life of the patient. Another method to treat ODRI is the use of antibiotic carriers which act as vehicles to release antibiotics locally in the surgical site. Although these carriers have shown promise, controlling the amount and release rate of antibiotics from these carriers over the short and long term remains a challenge.

In this study, I developed a coating that can be loaded with antibiotics and coated onto the surface of a 3D-printed titanium disc. The coating can release antibiotic slowly at normal body temperatures and more rapidly at higher temperatures. Just above body temperature, the polymer coating changes from a glassy state to a rubbery state allowing the release of antibiotic from the surface of the polymer into the surrounding environment. Higher temperatures were achieved using a device that emits a high frequency alternating magnetic field, which causes the surface of the titanium disc to heat without direct contact or heating the surrounding environment (e.g., the tissue) locally. We demonstrate that by using this heating device paired with an antibiotic-loaded coating we can either prevent or disrupt the formation of bacteria on the surface of metallic orthopedic devices which is where the infections are taking place.

Co-Authorship Statement

Chapter One was written by Jan C. Kwan and edited by Elizabeth R. Gillies.

Chapter Two is an original research article in preparation. Jan C. Kwan was involved as the main experientialist, interpreting the results, and manuscript preparation. Aneta Borecki, a research assistant in the Gillies laboratory, carried out the MTT assay experiments. David E. Heinrichs and Ronald S. Flannagan provided GFP expressing *S. aureus* and macrophages. David W. Holdsworth designed and aided in the construction of the induction heating unit. Karen Nygard at Biotron Integrated Microscope Facility at Western University helped with training and software support for all fluorescence imaging. Elizabeth R. Gillies as the supervisor designed the study, reviewed the results, provided editorial assistance, and mentorship. All of the contributors will be co-authors on the manuscript.

Chapter Three was written by Jan C. Kwan and edited by Elizabeth R. Gillies.

Acknowledgments

At the start, middle and end of my master's there have been a lot of ups and downs but even more importantly there are many individuals who have helped me on this journey. First, I want to thank Dr. Gillies, who saw my potential and took a chance on me. I am extremely appreciative of the constant support and mentorship she has provided me over the course of my master's. She has always been the first to tell it to you straight and can always turn a mistake or problem into a learning experience. Xueli was the first person I had met in the lab, and I couldn't be happier to have shared my lab bench with her. She is always willing to help and go beyond what is asked of her and has a great sense of humour while doing so. I cannot thank Monica enough for everything that she has done for me. She has been such a positive influence, a great friend, and an amazing lab mate. Her laughter fills the room and can always put a smile on anyone's face, and I am grateful for the effort she has put into helping me work on my experiments. I am also very glad that I had the opportunity to work alongside my friends Aneta, Andrew, Jared, Eric, Karan, Jay, Quinton, Xiaoli, Terry, and Joseph as they made my experience even more meaningful.

However, none of this could have been possible without my parents (Amy and Norman) who have always been my biggest supporters and continue to always push me to exceed my expectations. Without their continued support, I would not be where I am today and for that, I am forever grateful. The twins (Katelyn and Kay) have always been there for me when I need them most and are never afraid to share their thoughts. I can always count on them for their honesty, continued support and most importantly inspiring me to be a better person and brother. I would also like to thank Shania who has acted as an anchor and outlet for my frustration throughout my masters. She has been nothing short of supportive and caring and always willing to go the extra mile. She brings out the positive in any situation and I cannot express how lucky I am to have met this amazing person.

Table of Contents

Abstract.....	ii
Summary for Lay Audience.....	iii
Co-Authorship Statement.....	iv
Acknowledgments.....	v
Table of Contents.....	vi
List of Tables.....	ix
List of Figures.....	x
List of Schemes.....	xiv
List of Abbreviations.....	xv
Preface.....	xviii
Chapter 1.....	1
1 Introduction to orthopedic and trauma-related infections.....	1
1.1 Surgical implants and trauma-related devices.....	2
1.1.1 Prevalence and complications.....	3
1.1.2 Mechanism of biofilm development.....	4
1.2 Current available treatments for ODRI.....	5
1.2.1 Revision surgery and systemic antibiotic therapy.....	5
1.2.2 Antibiotic-eluting carriers.....	6
1.3 Antibacterial coatings.....	10
1.3.1 Definition and examples of antibacterial coatings.....	10
1.3.2 Definition and examples of antibiotic-eluting coatings.....	13
1.4 Inductive heating with an electromagnetic field.....	15
1.5 Poly(ester amides).....	18
1.5.1 Background.....	18

1.5.2	Thermal properties and biodegradability of PEAs.....	19
1.6	Thesis objectives.....	20
1.7	References.....	21
Chapter 2	30
2	Thermo-responsive antibiotic-eluting coatings for treating infection near orthopedic implants.....	30
2.1	Introduction.....	30
2.2	Experimental.....	34
2.2.1	General experimental details.....	34
2.2.2	Coating preparation.....	35
2.2.3	Thermal analysis of rifampicin-PEA blends.....	35
2.2.4	Scanning electron microscope (SEM)	35
2.2.5	<i>In vitro</i> release of rifampicin.....	36
2.2.6	<i>In vitro</i> degradation of coating in PBS	36
2.2.7	Induction heater design.....	37
2.2.8	Rifampicin release triggered by induction heating	38
2.2.9	Fibrinogen adsorption.....	39
2.2.10	Biofilm culture and growth conditions	39
2.2.11	Effect of different combinations of IH and antibiotics on <i>S. aureus</i> biofilm growth and the bacterial viability	40
2.2.12	Fluorescence microscopy of GFP-labeled <i>S. aureus</i> on coated discs.....	41
2.2.13	Live/dead analysis of <i>S. aureus</i> on coated discs	41
2.2.14	Mammalian cell viability	42
2.2.15	Statistical analysis.....	43
2.3	Results and discussion	43
2.3.1	Preparation and characterization of PEA coatings.....	43
2.3.2	<i>In vitro</i> release of rifampicin in the absence of the thermal triggering.....	45

2.3.3	Thermally triggered rifampicin release.....	48
2.3.4	Drug release induced by IH	49
2.3.5	Biofilm growth and <i>S. aureus</i> viability on Ti discs	51
2.3.6	Mammalian cell viability	57
2.3.7	Conclusions.....	58
2.4	References.....	59
Chapter 3	66
3	Summary and future work.....	66
3.1	References.....	69
Appendices	71
Appendix 1	– Supporting information for Chapter 2: Thermo-responsive Antibiotic-Eluting Coatings for Treating Infection near Orthopedic Implants	71
Appendix 2	– Permission to reuse copyrighted material	73
Curriculum Vitae	74

List of Tables

Table 1: Quantification of the bacterial biofilm for each treatment in a 48 h biofilm and CFU/mL calculation followed by a percent calculation of inhibited growth.	55
--	----

List of Figures

Figure 1.1: Stages of biofilm development beginning with the irreversible attachment of planktonic bacteria onto the substrate surface. An extracellular matrix forms around the micro-colonies until it reaches maturity. The mature biofilm then releases planktonic bacteria to disperse repeating a new cycle.³³ Figure readapted and reproduced with permission from Microbiology & Experimentation open access journal. 5

Figure 1.2: (A) Schematic of a total hip joint replacement using acrylic bone cement for implant fixation.⁵⁴ Figure reproduced from London: IntechOpen open access journal. (B) An intramedullary nail (top) and the same intramedullary nail wrapped in PMMA bone cement mixed with gentamycin (bottom).⁵⁵ Figure reproduced with permission from the author of reference 54..... 8

Figure 1.3: Readaptation of Athans et al.'s schematic of (A) combination of PMMA cement package and antibiotic powder. (B) Mixing of contents to create antibiotic-loaded bone cement. (C) Placement of antibiotic-loaded bone cement into the socket of the hip joint. (D) Fixation of the hip implant using PMMA bone cement and drug elution is represented by yellow arrows.⁵⁶ Figure reproduced with permission from reference 55. Copyright 2017, John Wiley and Sons. 8

Figure 1.4: A smooth paste of pharmaceutical-grade calcium sulfate alpha-hemihydrate mixed with vancomycin is pressed into 4.8 mm diameter hemispherical cavities in a flexible mould. (B) Antibiotic-loaded calcium sulfate beads were removed from the flexible mould after leaving it undisturbed for 30 – 60 minutes to set.⁶¹ Figure reproduced with permission from PLoS One open access journal. 9

Figure 1.5: Schematic diagram of PLL-g-PEG with a positively charged amino-terminated side chain bound to a negatively charged titanium oxide surface via multiple-site electrostatic interactions. Figure reproduced with permission from reference 65. Copyright 2003, Elsevier. 11

Figure 1.6: Schematic illustration of the antibacterial upper layer and the anti-fouling sub-layer and the chemical structure of the gemini quaternary ammonium salt waterborne

polyurethanes film. Figure reproduced with permission from Scientific Reports open access journal.	13
Figure 1.7: Schematic of the bioactive spherical nanoparticles anchored to Ti with gentamicin sulfate (GS) under neutral and acidic pH environments. Figure reproduced with permission from reference 80. Copyright 2012, Elsevier.	14
Figure 1.8: Schematic of the preparation of antibiotic-loaded coatings and their bacterial infection response in the presence of enzyme SplB cleaving vancomycin off the peptide. Figure reproduced with permission from reference 81. Copyright 2012, John Wiley and Sons.	15
Figure 1.9: Schematic illustration of the DOXO-loaded SPION with an attached folate factor. Figure reproduced with permission from reference 91. Permission conveyed through Copyright Clearance Center, Inc.	17
Figure 1.10: (A) 20 W delivered to solenoid coil at a frequency of 500 kHz controlled by a laptop and (B) fibre-optic temperature measurements of the washer's surface during 10 min AMF exposure. Figure reproduced with permission from Scientific Reports open access journal.	18
Figure 1.11: General chemical structure of a poly(ester amide).	19
Figure 2.1: Schematic showing a thermo-responsive drug-eluting PEA coating triggered by IH using an alternating magnetic field. The heating of the PEA above its T _g results in increased drug mobility and the release of rifampicin from the surface.	34
Figure 2.2: A) Frontal view of the induction device setup showing a solenoid coil (40 mm ID) wrapped around a 3D-printed PETG cylinder holding in place the PETG sample holder with the K-type thermocouple co-axially aligned with the Ti disc sample. B) The position of the Ti disc sample within the PETG sample holder.	37
Figure 2.3: A) Top view of the custom-made inductive heating device and B) Exploded view of a 3D-printed Ti disc sample at the center of a PETG sample holder with a K-type	

thermocouple in contact with the surface of the Ti disc and thermometer to measure the surrounding medium temperature. 38

Figure 2.4: DSC thermographs of pure PBSe and PBTe and their formulations with rifampicin. The incorporation of antibiotic led to modest increases in the T_g 45

Figure 2.5: Release of rifampicin from PEA containing A) 5% (w/w) and B) 10% (w/w) drug on Ti discs suspended in PBS at varying temperatures. More rapid release of drug occurred for the PBSe coatings but not for the PBTe coatings at elevated temperatures. Error bars correspond to the standard deviations on triplicate samples. 46

Figure 2.6: Degradation, based on mass loss, of PBSe coatings containing 5% (w/w) of rifampicin incubated in PBS at A) 37 °C for 105 days or B) temperatures ranging from 50 – 80 °C for three h. The coatings remained largely intact with minimal mass loss during each of these experiments. Error bars correspond to the standard deviations on triplicate samples. 47

Figure 2.7: Scanning electron micrographs of the surface of PBSe-rifampicin coatings (5% (w/w) drug) A) Prior to incubation; C) After incubation at 37 °C for 60 days; C) After incubation at 37 °C for 105 days; D) After incubation at 80 °C for 3h. 47

Figure 2.8: Release of rifampicin from PEA coatings containing A) 5% (w/w) and B) 10% (w/w) drug on Ti discs suspended in PBS at varying temperatures. More rapid release of drug occurred for the PBSe coatings but not for the PBTe coatings at elevated temperatures. Error bars correspond to the standard deviations on triplicate samples. 49

Figure 2.9: Release of rifampicin from inductively heated PBSe coatings on Ti discs using two different heat cycling procedures and compared to the same coatings without inductive heating, held at 37 °C. Error bars correspond to the standard deviations on triplicate samples. 51

Figure 2.10: Biofilm formation as measured by the crystal violet assay for *S. aureus* seeded on A) PBSe coatings with different combinations of antibiotic and IH; B) combinations of antibiotic and IH following treatment of PBSe coatings with fibrinogen, compared to no fibrinogen treatment. All treatments led to the suppression of biofilm formation, with a

combination of antibiotic and IH providing a large, synergistic effect both in the presence and absence of fibrinogen. All samples are normalized to untreated PBSe without IH or antibiotic (100% biofilm). All sample groups were statistically significantly different ($p < 0.05$, $N=3$). 52

Figure 2.11: Fluorescence microscopy of GFP-expressing *S. aureus* on Ti discs with A) PBSe coating alone; B) PBSe coating with IH treatment at 2 h and 24 h; C) PBSe coating containing 2.5% (w/w) of rifampicin; D) PBSe coating containing 2.5% (w/w) rifampicin and treated with IH at 2 and 24 h. Rifampicin-loaded PBSe coatings treated with IH led to the greatest suppression of GFP-expressing bacteria. 54

Figure 2.12: Fluorescence microscopy analysis of live and dead *S. aureus* on PBSe coated Ti discs with IH treatment at 2 h and 24 h, PBSe coating containing 2.5% (w/w) of rifampicin, and PBSe coating containing 2.5% (w/w) rifampicin and treated with IH at 2 and 24 h. Rifampicin-loaded PBSe coatings treated with IH led to the lowest population of live bacteria and the highest population of dead bacteria ratio. 55

Figure 2.13 The metabolic activity of macrophages was measured using an MTT assay to determine the viability of adhered macrophages on PEA coated and uncoated samples and subjected to one cycle of intermittent IH at 50 °C. All samples are normalized to the positive control, tissue-cultured well surface (100% metabolic activity). All sample groups were statistically significantly different ($p < 0.05$, $N=3$). 58

List of Schemes

Scheme 2.1: Chemical structure of A) PBSe and B) PBTe.....	44
--	----

List of Abbreviations

Ag	Silver
AMF	Alternating magnetic field
CFU	Colony forming units f
cm	Centimeter
Cm	Chloramphenicol
CV	Crystal violet
D	Dispersity
DAIR	Debridement antibiotic and implant retention
DCM	Dichloromethane
DI	Deionized water
DMEM	Dulbecco's modified eagle medium
DMF	Dimethylformamide
DMSO	Dimethyl sulfoxide
DOXO	Doxorubicin
EG-12	L-lysine derivatized diamine containing GQAS
EPS	Extracellular polymeric substance
Fe₂O₃	Ferric oxide
Fe₃O₄	Ferrous ferric oxide
FeO	Ferrous oxide
GFP	Green fluorescent protein
GQAS	Gemini quaternary ammonium salt
HA	Hydroxyapatite
HER-2	Human epidermal growth factor receptor 2

HPLC	High-performance liquid chromatography
IH	Induction heating
IPDI	Isophorone diisocyanate
LPS	Lipopolysaccharide
mg	Milligrams
MIC	Minimum inhibitory concentration
mL	Milliliters
M_n	Average molar mass
mol	Moles
MTT	3-(4,5-dimethylthiazol-2-yl)-2,5-diphenyl tetrazolium bromide
nm	Nanometer
ODRI	Orthopedic device-related infections
PBS	Phosphate buffered saline
PBSe	Phenylalanine, 1,4 butanediol, and sebacic acid
PBT_e	Phenylalanine, butanediol, and terephthaloyl chloride
PEA	Poly(ester amide)
PEG	Poly(ethylene glycol)
PI	Propidium iodide
PID	Proportional-integral derivative
PJI	Peri-prosthetic joint infection
PLL-g-PEG	Poly(L-lysine)-grafted-poly(ethylene glycol)
PMMA	Polymethyl methacrylate
PTMG	Polyoxytetramethylene glycol
QACs	Quaternary ammonium compounds
qCR-CSC	Quiescent colorectal cancer stem cells
SEM	Scanning electron microscope

SPIONs	Superparamagnetic iron oxide nanoparticles
SpIB	Serine protease-like protease
SSI	Surgical site infections
T_g	Glass transition temperature
THA	Total hip arthroplasty
Ti	Titanium
TKA	Total knee arthroplasty
T_m	Melting temperature
TSA	Tryptic soy agar
TSB	Tryptic soy broth
UV	Ultraviolet
W	Watts
W	Watts
w/w	Weight for weight
μL	Microliter

Preface

This work is dedicated in the memory of Ju Jin Shui.

Chapter 1

1 Introduction to orthopedic and trauma-related infections

The clinical use of orthopedic implants (hip or knee replacements) and trauma-related devices (nails, plates, or screws) to restore the function of joints has been well established as a reliable and effective treatment.¹⁻³ The demand for total knee and hip joint replacements and other orthopedic surgeries continues to rise. In Canada, the number of arthroplasties performed over the past five years has increased by 17%.⁴ In the United States (US), it is projected that by 2030 the demand for total hip arthroplasty (THA) procedures will grow by about 174% to 572,000 and total knee arthroplasty (TKA) procedures by around 673% to 3.48 million.⁵

Although major advancements have been made in the effectiveness of orthopedic surgical devices related to stronger biomaterials and reducing biomechanical failure, there has been a lack of development in resolving infection associated with orthopedic devices.⁶ Despite the best surgical management, prophylaxis, and the most stringent antiseptic protocols, infection is still an ongoing problem within the orthopedic field.⁷ When bacterial contamination of the surgical site from pathogens occurs it negatively impacts the clinical outcome of surgery in the short and long term for the patient. Infections in the orthopedic field are commonly defined as orthopedic device-related infections (ODRI).⁸ This term encompasses different types of infections which include peri-prosthetic joint infections (PJI) and orthopedic surgical site infections (SSI). PJI is defined as an infection followed by total joint arthroplasty involving the joint prosthesis and adjacent tissues more commonly seen in hip and knee replacements.⁹ Orthopedic SSIs occur post-surgery when the orthopedic device is contaminated at the time of implantation or when bacteria travel within the bloodstream and enter the surgical site from other locations of the patient's body. This is known as a process called hematogenous dissemination.¹⁰

The current standard of treatment for a patient who is diagnosed with an ODRI is revision surgery.⁸ Although there are different methods for performing a revision surgery such as one and two-stage revision surgery, amputation, debridement antibiotics and implant

retention (DAIR). The main purpose is to remove the infected device and clear the infection with the hopes of re-implantation of a new orthopedic device. Despite the high reported success of revision surgeries, many studies have indicated that there is a large economic burden on the healthcare system and a poor quality of life for patients recovering from revision surgery.^{7,8,11,12} On average, patients that undergo revision surgery require a longer hospitalized recovery time of approximately nine days as compared to only 3.8 days after primary surgery.^{7,11,12} Inpatient costs for revision surgery are also 70.2% (\$17,200) higher than the cost of primary surgery (\$10,000) in Canada.⁴ In Canada, nearly 10,000 hip and knee revision surgeries are performed each year with healthcare costs of around \$160 million (CAD), while in the United States healthcare expenditures related to these revision surgeries are projected to reach \$1.85 billion (USD) by 2030.^{11,13} Revision surgeries are also more complex than primary surgeries and can negatively affect the quality of life of the patient.^{7,12} Studies have also shown the potential for re-infection to be significantly greater than an initial infection after primary surgery.^{14,15}

The development of current antibiotic eluting carries such as poly(methyl methacrylate) (PMMA) bone cement and calcium sulfate and phosphate beads have helped the fight against ODRI by providing local antibiotic delivery to the infected site in conjunction with revision surgeries.¹⁶ In the past decade, the use of antibiotic carriers has gained considerable attention in the orthopedic field, but many studies have now shed light on their limitations in the ability to control drug release, disrupt biofilm formation and eradicate antibiotic-resistant bacteria.¹⁷

1.1 Surgical implants and trauma-related devices

In the orthopedic field, when a patient's joint can no longer function as intended due to injury or disease, it can be replaced completely with a surgical implant via a process called arthroplasty. Hip and knee replacements are among the most common elective surgeries for patients and many studies have reported their clinical efficacy with 82% and 58% of total knee and hip replacements lasting up to 25 years, respectively.¹⁸

While orthopedic trauma can be defined as severe injury to one or more organs or tissues in the musculoskeletal system it is often associated with joints, bones, muscles, and tendons. The most common causes of orthopedic traumas are car crashes and sports injuries.¹⁹ As a result, surgical treatment using trauma-related devices such as nails, plates, and screws is often necessary to restore the function of joints. For example, an open tibial fracture that is stabilized via an external fixation may use plates or an intramedullary nail.²⁰

Both surgical implants and trauma-related devices are commonly made from biomaterials that have high strength, tensile, compressive, and stiffness properties such as titanium alloys, stainless steel, cobalt-chromium, and alumina.²¹ This allows the devices to be load bearing, have low friction, and endure the high-stress environment within joints while lasting over the long term.²²

1.1.1 Prevalence and complications

There have been significant improvements in reducing the risk of biomechanical failure of surgical implants and trauma-related devices. However, high susceptibility to infection of these surgical devices remains, with very few solutions that have been validated by randomized control trials.²³ The incidence of infection varies from 0.7 – 4.2% for elective implant surgery and up to 30% in complex fractures for trauma surgeries.⁸ In elective implant surgery, the incidence of PJI has risen to 2.7% in the US and 1.6% in Canada.²⁴ For trauma-related surgeries, the rate of infection for internal fixation surgeries is approximately 1% but this number increases to a range of 15 – 55% in open fracture surgeries depending on the severity of the case.²⁵⁻²⁷

Despite the use of stringent antiseptic protocols or surgical management to maintain sterility at the infection site, orthopedic device-related infections still occur. The standard approaches are not sufficient as bacteria can still enter the surgical site from other areas of the body or through blood.¹⁰ Once bacteria have attached to a biomaterial surface, they can begin to proliferate and construct a protective environment called a biofilm. It is this biofilm that causes most of the complications that are suffered by the patient resulting in an infection that eventually leads to revision surgery.²⁸

1.1.2 Mechanism of biofilm development

The first phase of biofilm development happens when free-floating bacteria, or planktonic bacteria, have invaded the surgical site and come into contact with metal substrates, in a process known as reversible adherence. The second phase is defined as an irreversible attachment, which is initiated by bacteria fixing themselves onto the metal substrate surface via structural proteins called adhesins. The bacteria then begin to aggregate and develop an extracellular matrix onto the metal substrates.²⁹ In the third phase, an extracellular polymeric substance (EPS) made by bacteria can act as a scaffold for the biofilm to grow and undergo rapid cell division.³⁰ In the late stages of development, the biofilm continues to grow until it fully matures with micro-colonies merging into a sizeable three-dimensional structure. In the final stages, the micro-colonies and bacteria from the biofilm can detach to colonize other parts of the metal substrates that are unaffected to repeat the cycle.³¹ The types of bacteria that have been reported to be commonly associated with orthopedic device-related infections include *Staphylococcus aureus* (*S. aureus*) (20%-30%), *coagulase-negative staphylococci* (CoNS) (20%-40%), *Streptococci* (1%-10%), and *Enterococci* (3%-7%). However, the most notorious biofilm-forming bacterial species commonly associated with surgical implant and trauma-related devices are *Staphylococci*.⁸

Fully matured biofilms are complex microbiome structures composed of extracellular polymeric secretions made up of proteins, lipids, and polysaccharides (Fig 1.1).³² Provided with the ideal environmental conditions, biofilms can become very thick, ranging from 50 μm to 400 μm , and act as a barrier to the host's innate immune system. In addition, they can exhibit quorum sensing to control and restrict gene expression and induce an oxidatively stressed microenvironment with a low metabolic activity where persister bacteria lay dormant.¹⁴ The bacteria within a biofilm are diverse in their phenotypes and genotypes adding another layer of protection against antimicrobial agents. If left untreated, a combination of these elements prevents systemic antibiotic therapy from being effective and allows for the continued biofilm growth and the development of antibiotic-resistant bacteria on the surfaces of metal implants and trauma-related devices.⁹

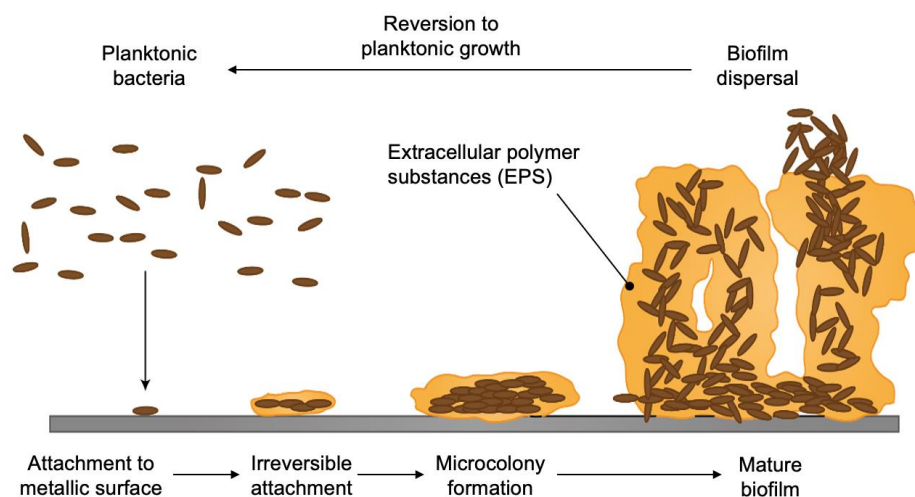


Figure 1.1: Stages of biofilm development beginning with the irreversible attachment of planktonic bacteria onto the substrate surface. An extracellular matrix forms around the micro-colonies until it reaches maturity. The mature biofilm then releases planktonic bacteria to disperse repeating a new cycle.³³ Figure readapted and reproduced with permission from Microbiology & Experimentation open access journal.

1.2 Current available treatments for ODR

1.2.1 Revision surgery and systemic antibiotic therapy

Revision surgery is a very common modality and is considered a standard treatment in patients that suffer from persistent ODR.³⁴ The most common method for performing revision surgery is either a one-stage or two-stage revision surgery. A one-stage revision surgery involves the removal of the infected device and surgical debridement, which is the removal of infected tissue while preserving any healthy tissue to improve healing, and implantation of a new device. A two-stage revision surgery involves the same steps as a one-stage, however after surgical debridement, a temporary cement spacer loaded with an antibiotic is implanted to serve as a placeholder, and then the wound is closed and allowed to heal. At this time, patients often undergo systemic or local antibiotic therapy and are monitored closely to ensure that the infection is completely cleared within the surgical site. After eight weeks, or when the infection has been cleared, a new device is implanted. Clinically, two-stage revision surgery is the most common standard treatment

in ODRI and has a reported success rate of up to 80%.³⁵ However, a more exhaustive review must be conducted, especially with more data from randomized controlled trials to understand the clinical outcomes of both one-stage and two-stage revision surgeries.³⁵

In some cases, two-stage revision surgery or systemic and local antibiotic therapy alone is ineffective in clearing the infection. Therefore, it is quite common for a combination of the two treatments to be used when treating ODRI.³⁶ During the healing phase of two-stage revision surgery, patients can receive systemic antibiotic therapy intravenously or orally to help treat the infection, the most common are Cefazolin, Vancomycin and Penicillin.³⁷ However, these methods may not be entirely effective as antibiotics are often unable to eradicate an established mature biofilm and may potentially induce antibiotic resistance in bacteria.³⁸ Systemic antibiotic treatment may require antibiotic concentrations that would exceed the toxic threshold for patients to resolve these types of infections.³⁹ To address this challenge, following surgical debridement in two-stage revision surgery, the temporary cement spacer can be used as an antibiotic carrier, typically in the form of acrylic bone cement. Additionally, calcium sulfate or phosphate beads loaded with antibiotics can also help release antibiotics locally to assist in eradicating the infection during the healing phase before the implantation of a new device.^{35,36,39,40}

1.2.2 Antibiotic-eluting carriers

Antibiotic-eluting carriers are drug delivery systems that exhibit antibacterial activity by eluting drugs continuously over time in the local environment of the orthopedic device to prevent biofilm formation and infection.⁴¹⁻⁴³ The use of local antibiotic-eluting carriers has been well documented as a method for treating ODRI since the late 1970s.^{39,44} One of the first methods of local drug delivery was introduced by Buchholz and Engelbrecht, who employed PMMA bone cement spacers containing gentamycin utilized as temporary implant placeholders during the healing stage of two-stage revision surgery before the implantation of the new device.⁴⁴ In the past decade, the use of antibiotic-eluting carriers has gained considerable attention in the orthopedic field. Currently, PMMA, calcium sulfate, and calcium phosphate are used as drug delivery materials in the treatment of

ODRI. However, new studies have shed light on limitations in their abilities to control drug release, disrupt biofilm formation, and eradicate antibiotic-resistant bacteria.⁴⁵

The initial use of PMMA was for structural support and fixation of implants to maintain stability or to maintain the joint space after removal of the primary device, in which case it is also referred to as a bone cement spacer (Fig 1.2).⁴⁶ Antibiotics can be added to the pre-polymerized PMMA formulation, allowing for high local antibiotic concentrations in the surgical site post-operatively (Fig 1.3). Although PMMA is a widely used antibiotic carrier in the orthopedic field, it has several drawbacks. Antibiotics that are temperature sensitive cannot be combined with PMMA as it undergoes an exothermic polymerization reaction and can generate very high temperatures. Aminoglycosides are typically used with PMMA when compared to other antibiotics as they can withstand high temperatures.⁴⁷ The amount of drug-loaded relative to PMMA is also limited. At most, 1 g of antibiotic per 40 g of cement package is recommended based on the manufacturer's instructions, so as to not compromise the mechanical strength of the cement.^{41,48} Studies have investigated the effects of adding more than the recommended antibiotic amount, concluding that improved drug release could be achieved but a decrease in compressive strength of the cement was observed.⁴⁹ PMMA bone cement has also been found to be effective in killing bacteria only in the first few hours post-operatively and a release of sub-inhibitory antibiotic concentrations was obtained for several days thereafter.⁵⁰ Furthermore, as PMMA bone cement is non-biodegradable, in cases of septic loosening of the implant, the bone cement must be completely removed to clear infection as the surface of PMMA can be colonized by planktonic bacteria that could develop into a biofilm rather quickly.⁵¹ In trauma surgery for open tibial fractures, PMMA and antibiotic-coated nails have been regularly used but have the same reported limitations (Fig 1.2).⁵² However, there have been now many reports cautioning antibiotic choice when using PMMA bone cement as a carrier due to the emergence of aminoglycoside-resistant bacteria.⁵³

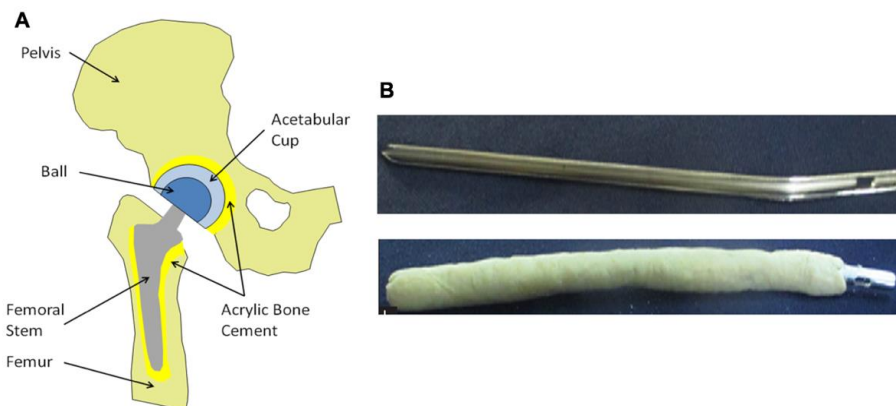


Figure 1.2: (A) Schematic of a total hip joint replacement using acrylic bone cement for implant fixation.⁵⁴ Figure reproduced from London: IntechOpen open access journal. (B) An intramedullary nail (top) and the same intramedullary nail wrapped in PMMA bone cement mixed with gentamycin (bottom).⁵⁵ Figure reproduced with permission from the author of reference 54.

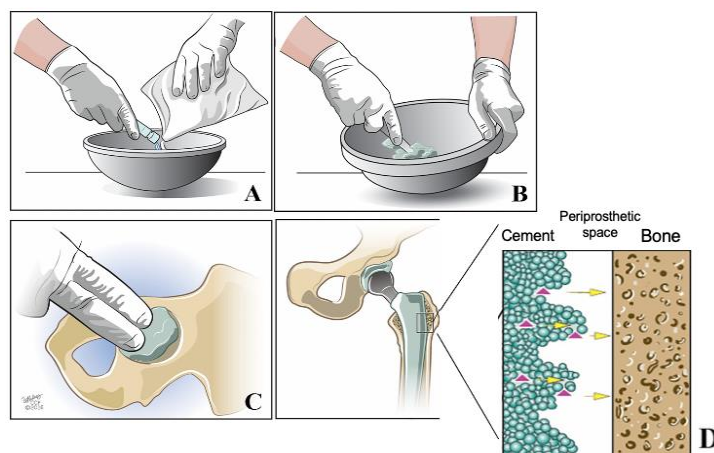


Figure 1.3: Readaptation of Athans et al.'s schematic of (A) combination of PMMA cement package and antibiotic powder. (B) Mixing of contents to create antibiotic-loaded bone cement. (C) Placement of antibiotic-loaded bone cement into the socket of the hip joint. (D) Fixation of the hip implant using PMMA bone cement and drug elution is represented by yellow arrows.⁵⁶ Figure reproduced with permission from reference 55. Copyright 2017, John Wiley and Sons.

In recent years, there has been a shift towards the clinical use of resorbable materials such as calcium sulfate and calcium phosphate as drug delivery systems.⁵⁷ These carriers are commonly referred to as bone void filler beads and unlike PMMA can be completely absorbed within the body. The method of antibiotic encapsulation is like that of PMMA (Figure 1.4).⁵⁸ These carriers can reside in the body for about 4 -13 weeks and can be combined with a much wider range of antibiotics.^{45,50} During this period, they typically release their entire antibiotic load with an initial burst release in the first several days. Many studies have concluded that there is a much faster drug release using these carriers than PMMA bone cement and as a result a higher efficacy in treating ODRI.^{49,59} However, drug release varies and is dependent on the amount of antibiotic-loaded in these carriers. The antibiotic can also affect the rate of degradation. Higher antibiotic concentrations within these beads result in longer elution periods but can compromise mechanical strength, resulting in an increased rate of degradation.⁵⁹ Overall, obtaining the ideal amount of antibiotics in these carriers for both the short and long term to prevent and destroy biofilms and consistently elute inhibitory antibiotic concentrations remains a challenge.⁶⁰

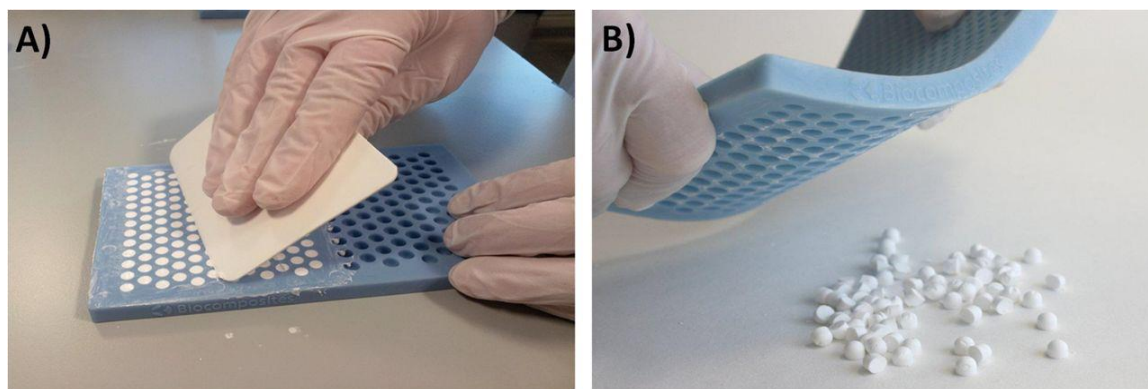


Figure 1.4: A smooth paste of pharmaceutical-grade calcium sulfate alpha-hemihydrate mixed with vancomycin is pressed into 4.8 mm diameter hemispherical cavities in a flexible mould. (B) Antibiotic-loaded calcium sulfate beads were removed from the flexible mould after leaving it undisturbed for 30 – 60 minutes to set.⁶¹ Figure reproduced with permission from PLoS One open access journal.

1.3 Antibacterial coatings

1.3.1 Definition and examples of antibacterial coatings

Antibacterial coatings have been explored in many different applications and have also been a key research area that has shaped the understanding of treating infection and the prevention of biofilm formation on orthopedic devices.⁶² Antibacterial coatings can work in two ways, either passively or actively.

Passive antibacterial coatings can hinder the ability of bacterial attachment or kill bacteria upon contact. As a result, bacteria have a difficult time adhering to the surfaces of these coatings and decreasing the chance of biofilm formation. Different physical and chemical properties of these coatings have been used to reduce bacterial adhesion. For example, studies have used polymers such as poly (ethylene glycol) coated onto titanium (Ti) surfaces being able to inhibit bacterial adhesion.^{63,64} Harris and colleagues took this one step further and investigated *S. aureus* adhesion on non-functionalized and peptide-functionalized poly(L-lysine)-grafted-poly(ethylene glycol) (PLL-g-PEG) coatings on Ti surfaces (Figure 1.5).⁶⁵ The authors concluded reduced surface adhesion of *S. aureus* to 89-93%, however, upon functionalization of PLL-g-PEG with peptides RGD (Arg-Asp-Gly) the coating was able to attach to fibroblasts and osteoblasts to a higher degree when compared to non-functionalized PLL-g-PEG while still reducing *S. aureus* adhesion to about 69%. Other strategies of passive antibacterial coatings include antifouling mechanisms which include coating biomedical devices with hydrophilic, hydrophobic, or zwitterionic polymers or surface modifications which include roughness, wettability, and topography against bacteria colonization which have all shown success.⁶⁶ Additionally, the advantage of passive coatings is that they do not induce bacterial resistance, but the disadvantage is that their antibacterial efficacy varies and can be weak depending on the bacteria strain.⁶⁷

agents.^{70,71} Non-metals such as iodine have also been used as antibacterial agents.⁷² These coatings release free iodine and can penetrate bacterial cell walls and kill via iodination of lipids and oxidation of key proteins, leading to eventual cell death. Lastly, organic compounds have also been used as antibacterial agents particularly ammoniums and antibiotics such as vancomycin and gentamicin have been used in preventing bacterial adhesion.⁷³⁻⁷⁵

The structure and components of a bacterial cell wall for gram-positive and gram-negative bacteria are different. Gram-negative bacteria have a unique outer membrane structure called lipopolysaccharide (LPS) and it functions as a barrier and is negatively charged to help stabilize the bacteria cell membrane. Gram-positive bacteria instead have teichoic acids which function to provide flexibility to the bacterial cell membrane and attract cations such as calcium and potassium along with a thick peptidoglycan layer. As a result, the bacterial cell walls for both types of bacteria are anionic, and researchers have been able to use this to their advantage in developing antibacterial agents with qualities that can have electrostatic interactions that disrupt the cell membrane and ultimately kill bacteria.⁷⁶ Ammonium compounds have been widely used in antibacterial coatings due to their mechanism of killing bacteria.⁷⁷ Particularly quaternary ammonium compounds have been reported to be more potent cationic antimicrobials when compared to tertiary and primary amines. Lia and colleagues investigated tethering quaternary ammonium compounds onto hyperbranched polyurea coatings for the killing of *Staphylococcus epidermidis* (*S. epidermidis*).⁷⁸ The authors observed contact killing of > 99.99% as a result of the strong adhesion forces between the hyperbranched quaternary ammonium coating and bacteria disrupting bacterial membrane lipids leading to cell death. Another example is an investigation by He and colleagues where they used gemini quaternary ammonium salt (GQAS) waterborne polyurethanes to develop a dual-layered coating with an antibacterial upper layer and an anti-fouling sub-layer.⁷⁹ The investigators had purposely chosen the order in layers due to the accumulation of dead cells and other proteins that could potentially mask the effects of the contact-active antibacterial coating. The design of the coating involved the use of a series of gemini waterborne polyurethanes synthesized using isophorone diisocyanate (IPDI), polyoxytetramethylene glycol (PTMG), PEG, L-lysine, and an L-lysine derivatized

diamine containing GQAS (EG-12). The gemini quaternary ammonium salt brushes were positioned above PEG and an anionic carboxylate layer (Fig 1.6). Their results showed a killing efficiency of 99.99% for both gram-positive and gram-negative bacteria.

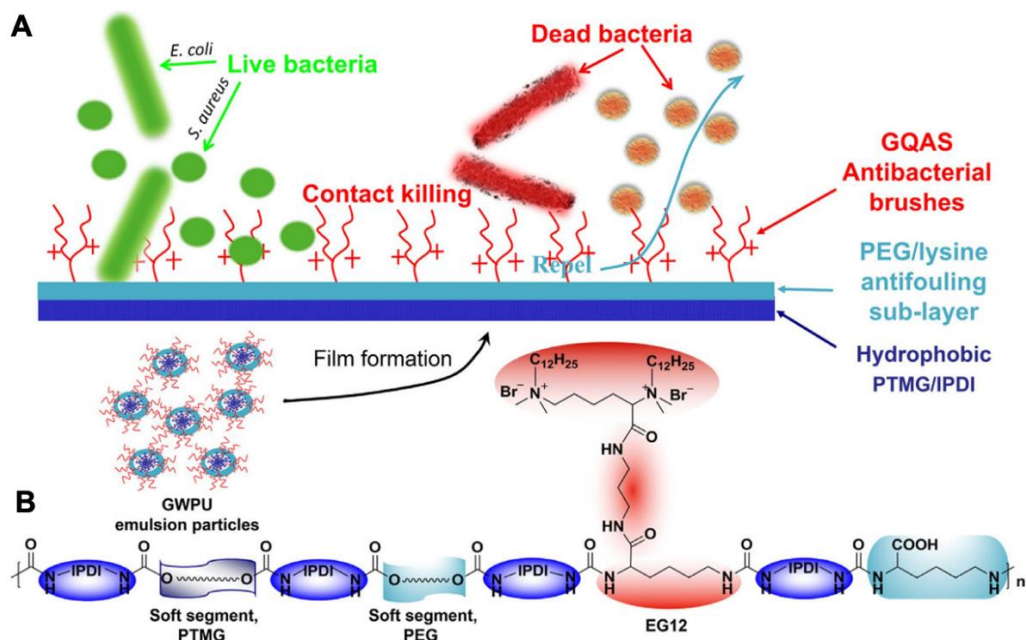


Figure 1.6: Schematic illustration of the antibacterial upper layer and the anti-fouling sub-layer and the chemical structure of the gemini quaternary ammonium salt waterborne polyurethanes film. Figure reproduced with permission from Scientific Reports open access journal.

1.3.2 Definition and examples of antibiotic-eluting coatings

In recent years, researchers have sought to develop smart degradable coatings and nanoparticles to prevent and treat the growth of biofilms on the metallic surfaces of medical devices non-invasively and in the presence of various factors associated with infection.⁸⁰ Different mechanisms in smart coatings and nanoparticles to trigger drug release have been explored. The main triggers include pH, bacterial by-products, and temperature.

Studies have investigated using low pH (4.0 – 5.0) as an active trigger for drug release. Pichavant and colleagues observed the controlled release of gentamicin sulfate using spherical nanoparticles chemically anchored to the surface of titanium (Ti) with the help

of the acidic pH in the local environment during infection.⁸¹ As a result of the acidic environment, this initiates the cleavage of the chemical bond between the nanoparticle and antibiotic, inducing drug release (Fig 1.7). The *in vitro* drug release result indicated that at an acidic pH of 4-5 a high initial release rate was observed, followed by a slower release rate over one week. However, at a pH of 7, there was no significant release of the drug observed. They reported significant inhibition of *S. epidermis* at 10^5 colony forming units (CFU) and a decrease in the minimum inhibitory concentration (MIC) at pH 6, 5, and 4.

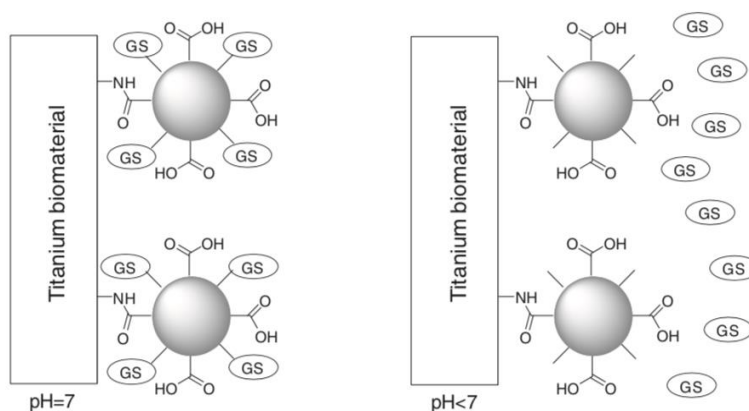


Figure 1.7: Schematic of the bioactive spherical nanoparticles anchored to Ti with gentamicin sulfate (GS) under neutral and acidic pH environments. Figure reproduced with permission from reference 80. Copyright 2012, Elsevier.

Zhang and colleagues took a novel approach using an enzyme secreted by *S. aureus* to trigger drug release.⁸² They used vancomycin covalently conjugated to a tailor-made peptide, GSWELQSGSGSC also known as SRP-1, that can be recognized and hydrolyzed by an enzyme that is secreted by *S. aureus* called serine protease-like protease (SplB) with enzymatic sites located at the Gln-Gly (Q-G) residues on a Ti surface (Fig 1.8). The results showed that Ti-SRP-Van, in the presence of excess SplB, an inhibitory rate of 67% was observed compared to 36% that was observed with Ti-SRP-Van in a normal culture of *S. aureus* in a 24h period. The strong antimicrobial activity was further confirmed with the same conditions in a 48 h period with an inhibitory rate of 86% and

82%, respectively, indicating antibacterial activity that is time-dependent demonstrating an infection-dependent drug release mechanism from the coating.

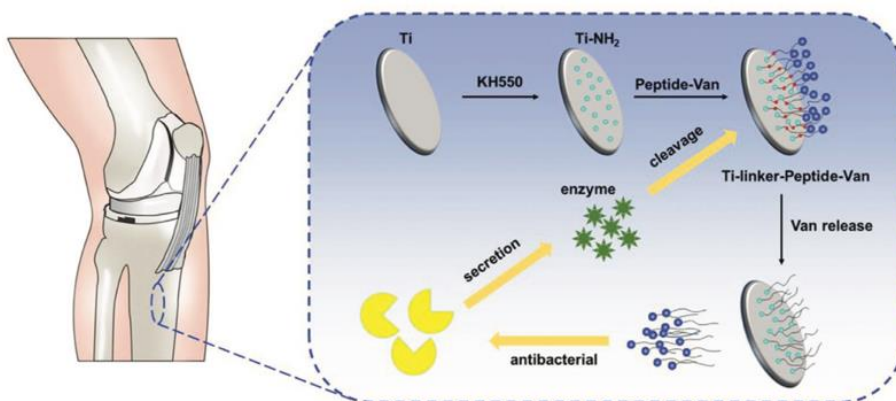


Figure 1.8: Schematic of the preparation of antibiotic-loaded coatings and their bacterial infection response in the presence of enzyme SplB cleaving vancomycin off the peptide. Figure reproduced with permission from reference 81. Copyright 2012, John Wiley and Sons.

1.4 Inductive heating with an electromagnetic field

Induction heating is defined as the process of electrically heating conductive materials such as metal alloys using an electromagnetic field that is generated near a coil. An induction heater can generate a high frequency alternating magnetic current, or an eddy current, which can penetrate the conductive material and produce an electric current from within.⁸³ A conductive material such as a titanium disc placed within the center of the coil can generate heat without using an external heat source that is in contact with the sample, allowing objects to be heated in a matter of seconds.⁸⁴ Induction heating applications span many fields including industrial processes such as welding and manufacturing and within the medical field such as sealing and cooking.⁸⁵

The medical use of induction heating has always been an interest in the field of cancer therapy.⁸⁶ The clinical application of induction heating is better described as magnetic hyperthermia and its main goal is to non-invasively increase a tumour's temperature to kill cancer cells and act as an adjuvant to radiation and chemotherapy.^{87,88} With the

advent of magnetic nanoparticles this concept of induction heating has been taken one step further by researchers in the field of cancer therapy with the ability of these nanoparticles to be triggered by an external magnetic field for cell-targeting, drug delivery or thermal ablation all while being well tolerated by the body.⁸⁸ The most common magnetic nanoparticles are iron oxides such as ferrous oxide (FeO), ferric oxide (Fe₂O₃), and ferrous ferric oxide (Fe₃O₄).⁸⁹ These magnetic nanoparticles can be further modified with improved selectivity and anti-tumour efficacy by attaching inorganic, organic or functionalized ligands for improved cell-targeting specificity or controlled drug delivery.⁹⁰ An example of this mechanism is an *in vitro* breast cancer study, where researchers used superparamagnetic iron oxide nanoparticles (SPIONs) to target breast cancer cells over-expressing human epidermal growth factor receptor 2 (HER2).⁹¹ Poly(acrylic acid) coated SPIONs with dye labelled anti-HER2 antibodies attached to the surface were used. The attached HER2 antibodies acted as a vehicle for the SPIONs to find and target high-specificity HER2 overexpressing tumour cells and were subsequently exposed to low magnetic field strength and a frequency of 400 kHz leading to a prominent decrease in breast cancer cell proliferation. SPIONs have also been extensively studied as a vehicle for drug delivery of doxorubicin (DOXO), one investigation loaded DOXO onto negatively charged polycarboxylic iron-oxide nanoparticles in the targeting of breast carcinoma cell lines.⁹² Whereas another study, researchers investigated DOXO-loaded SPIONs by an emulsion solvent preparation and attaching a folate factor to the nanoparticles using a folate-conjugated alginate to help the nanoparticle to enter and stay within the tumour cells of lung cancer-bearing mice (Fig 1.9).⁹³ Fernandes and colleagues investigated an iron oxide nanocube drug delivery vehicle coated with a thermo-responsive polymer loaded with and without doxorubicin (DOXO), a chemotherapeutic agent, to target quiescent colorectal cancer stem cells (qCR-CSC).⁹⁴ The authors concluded that magnetic hyperthermia initially caused qCR-CSCs to become stressed and induce cell division but at the same time, the increased temperature facilitated DOXO diffusion from the iron nanocubes into the cells making them more sensitive to DOXO. As a result, they were able to successfully eradicate qCR-CSC and avoid tumour relapse.

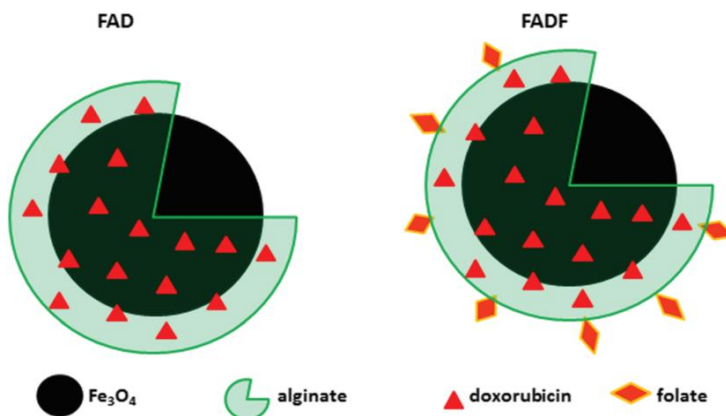


Figure 1.9: Schematic illustration of the DOXO-loaded SPION with an attached folate factor. Figure reproduced with permission from reference 91. Permission conveyed through Copyright Clearance Center, Inc.

In the orthopedic field, non-contact heating of metallic substrates potentially allows for a non-invasive treatment approach compared to the conventional method of revision surgeries in treating ODRI.^{95,96} Due to the mechanism of induction heating, any metallic orthopedic device can be heated whereas the surrounding tissue will not experience any direct heating.⁹⁷ The heat generated from within the metal device would result in an increased surface temperature where biofilms generally reside. However, the main reported limitations of induction heating in the orthopedic field have been tissue necrosis, the required duration of induction heating, and heating uniformity of complex shapes. The main concern is the viability of the tissue layer that is nearest to the surface of the metallic device that is being heated.⁸⁴ Pijls and colleagues used the concept of induction heating and attempt to reduce bacterial load on the surface of titanium alloy cylinders.⁹⁵ In their *in vitro* study investigating the effects of induction heating (2000 watts (W) at 27kHz) on planktonic bacteria they were able to observe a 5-log reduction for five different bacterial micro-organisms, including *S. aureus*, by heating at 60 °C for 1.5 minutes.

Another very relevant study by Chopra and colleagues used a very similar method of induction heating with a high frequency alternating magnetic field (AMF) > 100 kHz to target the biofilm.⁹⁸ The authors observed that exposing a stainless-steel washer to 20 W

for a continuous 10 min attained a surface temperature of around 90 °C at the 6-min mark (Fig 2.0). Results from an *in vitro* antibacterial experiment showed disruption of the biofilm matrix within 1 min of AMF followed by a > 5-log reduction CFU of *P. aeruginosa* and *S. aureus* after 5 min of AMF exposure. In their *in vivo* experiments, the authors instead employed an intermittent exposure of an AMF to a metal ball implanted in the dorsal thigh muscle of a mouse model with minimal thermal damage to the muscle fibers, connective tissue, and vascular channels. However, it was observed that damage was localized to areas less than 2 mm around the entire implant and only 1 mm when exposed to a reduced AMF of 800 W for 15 seconds. Although induction heating alone can prevent biofilm formation or destroy an established biofilm it seems that a high amount of power and AMF is still required to effectively target the biofilm and in almost all studies these requirements cannot be translated clinically in the context of safety for the patient.

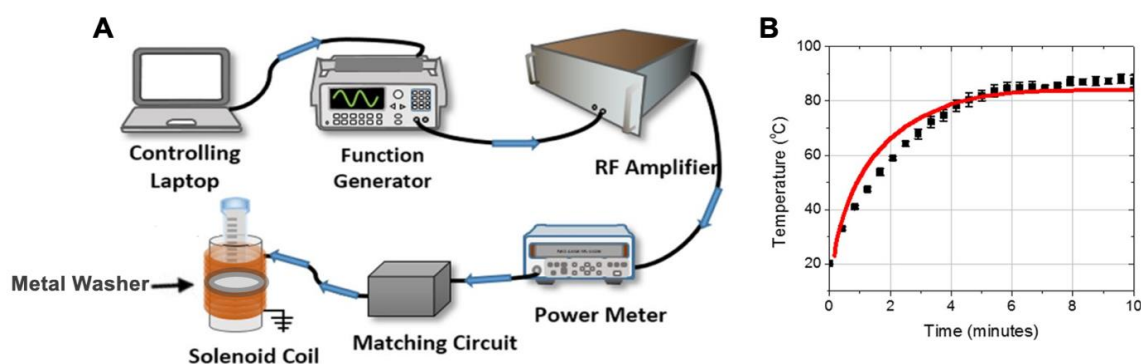


Figure 1.10: (A) 20 W delivered to solenoid coil at a frequency of 500 kHz controlled by a laptop and (B) fibre-optic temperature measurements of the washer's surface during 10 min AMF exposure. Figure reproduced with permission from Scientific Reports open access journal.

1.5 Poly(ester amides)

1.5.1 Background

Poly(ester amides) (PEAs) are a class of emerging synthetic biodegradable polymers that contain both ester and amide linkages within their backbones (Fig. 2.1). The amide

linkages allow for enzymatic degradation, while ester linkages can undergo degradation through enzymatic and non-enzymatic hydrolysis.⁹⁹ The popularity of PEAs is largely attributed to their tunable thermal, mechanical, and biocompatible properties.¹⁰⁰ PEAs can be functionalized by the incorporation of amino acids and other pendant side chains to elicit specific properties for certain biomedical uses. PEAs also have a wide range of biomedical applications including biodegradable hydrogels as drug carriers, porous 3D tissue scaffolds, dental composites/adhesives, tissue regeneration in joints, and drug delivery systems.^{101–105}

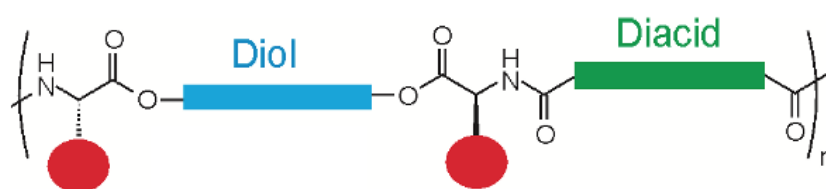


Figure 1.11: General chemical structure of a poly(ester amide).

1.5.2 Thermal properties and biodegradability of PEAs

When the surrounding temperature of a polymer increases, the polymer can be affected in several ways. One of the thermal properties of a polymer is its glass transition temperature (T_g) defined as the temperature where a polymer transitions from a glassy state into a viscous/rubbery state. Many polymers are amorphous and crystalline and have both a T_g and melting temperature (T_m), with the T_m being defined as the temperature where the crystalline domains of the polymer melt, T_g will always be lower than the T_m .¹⁰⁶ PEAs are attractive, as their thermal properties can be tuned depending on the chemical composition of the backbone. The incorporation of rigid monomers into the backbone has been shown to increase the T_g of PEAs.¹⁰⁷

Unlike many polyesters, PEAs tend to degrade not by bulk degradation, but rather by surface erosion, which is favorable in terms of retaining the structure and properties of the implanted material. In addition, a PEA amino acid-based composition limits the potential for degraded particles to induce systemic toxicity within the body.¹⁰⁸ Generally, PEAs have some commonalities in chemical composition with peptides and proteins.¹⁰⁹

As a result, PEAs have been reported to be well tolerated in different applications such as intra-articular drug delivery in the form of particles and ocular implants in the form of microfibrils.^{103,110,111} Overall, the tunable properties of PEAs allow for a multitude of biomedical applications, especially in drug delivery systems.¹⁰⁹ According to the best of our knowledge and literature reviews, no studies have investigated the combined use of induction heating and the T_g of a PEA to trigger drug release.

1.6 Thesis objectives

To the best of our knowledge, the use of a thermo-responsive polymer coating with induction heating has not yet been used to trigger the release of drugs. Thus, the main objective of this thesis is to develop a drug-eluting polymer coating for metal implants that can be thermally triggered by high-frequency alternating electromagnetic fields to release antibiotics rapidly at elevated temperatures to prevent and disrupt biofilm formation and infection in a controlled manner. It is anticipated that this antibiotic release may provide an additive or even synergistic effect in combination with the inductive heating of the implant surface.

1.7 References

1. Joung, Y.-H. INJ Development of Implantable Medical Devices: From an Engineering Perspective. *International Neurology Journal* (2013).
2. Räsänen, P. *et al.* Effectiveness of hip or knee replacement surgery in terms of quality-adjusted life years and costs. *Acta Orthop* **78**, 108–115 (2007).
3. Long, P. H. Medical Devices in Orthopedic Applications. *Toxicologic Pathology* **36**, 85–91 (2008).
4. CJRR annual report: Hip and knee replacements in Canada | CIHI. <https://www.cihi.ca/en/cjrr-annual-report-hip-and-knee-replacements-in-canada>.
5. Kurtz, S., Ong, K., Lau, E., Mowat, F. & Halpern, M. Projections of primary and revision hip and knee arthroplasty in the United States from 2005 to 2030. *J Bone Joint Surg Am* **89**, 780–785 (2007).
6. Boddapati, V. *et al.* Revision Total Knee Arthroplasty for Periprosthetic Joint Infection Is Associated With Increased Postoperative Morbidity and Mortality Relative to Noninfectious Revisions. *J Arthroplasty* **33**, 521–526 (2018).
7. Kamath, A. F. *et al.* Quantifying the Burden of Revision Total Joint Arthroplasty for Periprosthetic Infection. *J Arthroplasty* **30**, 1492–1497 (2015).
8. Moriarty, T. F. *et al.* Orthopaedic device-related infection: current and future interventions for improved prevention and treatment. *EFORT Open Rev* **1**, 89–99 (2017).
9. Tande, A. J. & Patel, R. Prosthetic Joint Infection. *Clinical Microbiology Reviews* **27**, 302 (2014).
10. Ellis, S. & Ong, E. Disseminated Infections: A Clinical Overview. *Molecular Medical Microbiology* 637 (2015).
11. Premkumar, A. *et al.* Projected Economic Burden of Periprosthetic Joint Infection of the Hip and Knee in the United States. *J Arthroplasty* **36**, 1484-1489.e3 (2021).
12. Bhandari, M., Smith, J., Miller, L. E. & Block, J. E. Clinical and economic burden of revision knee arthroplasty. *Clin Med Insights Arthritis Musculoskelet Disord* **5**, 89–94 (2012).
13. Hip and Knee Replacements in Canada, 2017–2018: Canadian Joint Replacement Registry Annual Report. (2019).
14. Chiu, F. Y. & Chen, C. M. Surgical débridement and parenteral antibiotics in infected revision total knee arthroplasty. *Clin Orthop Relat Res* **461**, 130–135 (2007).

15. Amerstorfer, F. *et al.* Risk of reinfection after two- or multiple-stage knee revision surgery using superficial vancomycin coating and conventional spacers. *Journal of Orthopaedic Research* **39**, 1700 (2021).
16. Metsemakers, W. J. *et al.* Evidence-Based Recommendations for Local Antimicrobial Strategies and Dead Space Management in Fracture-Related Infection. *J Orthop Trauma* **34**, 18–29 (2020).
17. Spitzmüller, R. *et al.* Duration of antibiotic treatment and risk of recurrence after surgical management of orthopaedic device infections: A multicenter case-control study. *BMC Musculoskeletal Disorders* **20**, 1–10 (2019).
18. Evans, J. T. *et al.* How long does a knee replacement last? A systematic review and meta-analysis of case series and national registry reports with more than 15 years of follow-up. *The Lancet* **393**, 655–663 (2019).
19. Soleymanha, M., Mobayen, M., Asadi, K., Adeli, A. & Haghparast-Ghadim-Limudahi, Z. Survey of 2582 Cases of Acute Orthopedic Trauma. *Trauma Monthly* **19**, 20–23 (2014).
20. Bhandari, M., Zlowodzki, M., Tornetta, P., Schmidt, A. & Templeman, D. C. Intramedullary nailing following external fixation in femoral and tibial shaft fractures. *J Orthop Trauma* **19**, 140–144 (2005).
21. Navarro, M., Michiardi, A., Castaño, O. & Planell, J. A. Biomaterials in orthopaedics. *Journal of the Royal Society Interface* **5**, 1137 (2008).
22. Huzum, B. *et al.* Biocompatibility assessment of biomaterials used in orthopedic devices: An overview (Review). *Experimental and Therapeutic Medicine* **22**, 1–9 (2021).
23. Haddad, F. S., Sukeik, M. & Alazzawi, S. Is single-stage revision according to a strict protocol effective in treatment of chronic knee arthroplasty infections? *Clin Orthop Relat Res* **473**, 8–14 (2015).
24. Kim, H. S. *et al.* Current and Future Burden of Periprosthetic Joint Infection from National Claim Database. *J Korean Med Sci* **35**, (2020).
25. Li, J. *et al.* Relationship Between Time to Surgical Debridement and the Incidence of Infection in Patients with Open Tibial Fractures. *Orthopaedic Surgery* **12**, 524 (2020).
26. Morgenstern, M. *et al.* Diagnostic challenges and future perspectives in fracture-related infection. *Injury* **49 Suppl 1**, S83–S90 (2018).
27. Trampuz, A. & Zimmerli, W. Diagnosis and treatment of infections associated with fracture-fixation devices. *Injury* **37 Suppl 2**, (2006).

28. Veerachamy, S., Yarlagadda, T., Manivasagam, G. & Yarlagadda, P. K. Bacterial adherence and biofilm formation on medical implants: a review. *Proc Inst Mech Eng H* **228**, 1083–1099 (2014).
29. Vigeant, M. A. S., Ford, R. M., Wagner, M. & Tamm, L. K. Reversible and irreversible adhesion of motile *Escherichia coli* cells analyzed by total internal reflection aqueous fluorescence microscopy. *Appl Environ Microbiol* **68**, 2794–2801 (2002).
30. Rabin, N. *et al.* Biofilm formation mechanisms and targets for developing antibiofilm agents. *Future Med Chem* **7**, 493–512 (2015).
31. McConoughey, S. J. *et al.* Biofilms in periprosthetic orthopedic infections. *Future Microbiol* **9**, 987–1007 (2014).
32. Schuster, J. J. & Markx, G. H. Biofilm architecture. *Advances in Biochemical Engineering/biotechnology* **146**, 77–96 (2014).
33. Vasudevan, R. Biofilms: microbial cities of scientific significance. *Journal of Microbiology & Experimentation* **Volume 1**, (2014).
34. Darouiche, R. O. Treatment of infections associated with surgical implants. *N Engl J Med* **350**, 1422–1429 (2004).
35. Charette, R. S. & Melnic, C. M. Two-Stage Revision Arthroplasty for the Treatment of Prosthetic Joint Infection. *Curr Rev Musculoskelet Med* **11**, 332–340 (2018).
36. Srivastav, A. K., Nadkarni, B., Srivastav, S., Mittal, V. & Agarwal, S. Prophylactic use of antibiotic-loaded bone cement in primary total knee arthroplasty: Justified or not? *Indian Journal of Orthopaedics* **43**, 259 (2009).
37. de Beer, J. *et al.* Antibiotic prophylaxis for total joint replacement surgery: results of a survey of Canadian orthopedic surgeons. *Canadian Journal of Surgery* **52**, E229 (2009).
38. Mirza, Y. H., Tansey, R., Sukeik, M., Shaath, M. & Haddad, F. S. Suppl-2, M6: Biofilm and the Role of Antibiotics in the Treatment of Periprosthetic Hip and Knee Joint Infections. *The Open Orthopaedics Journal* **10**, 636 (2016).
39. Elson, R. A., Jephcott, A. E., McGeachie, D. B. & Verettas, D. Antibiotic-loaded acrylic cement. *J Bone Joint Surg Br* **59**, 200–205 (1977).
40. Ricciardi, B. F. *et al.* New Developments and Future Challenges in Prevention, Diagnosis, and Treatment of Prosthetic Joint Infection. *J Orthop Res* **38**, 1423 (2020).

41. Gasparini, G. *et al.* Drug elution from high-dose antibiotic-loaded acrylic cement: a comparative, in vitro study. *Orthopedics* **37**, e999–e1005 (2014).
42. Webb, J. C. J. & Spencer, R. F. The role of polymethylmethacrylate bone cement in modern orthopaedic surgery. *J Bone Joint Surg Br* **89**, 851–857 (2007).
43. Boelch, S. P. *et al.* Comparison of Elution Characteristics and Compressive Strength of Biantibiotic-Loaded PMMA Bone Cement for Spacers: Copal® Spacem with Gentamicin and Vancomycin versus Palacos® R+G with Vancomycin. *Biomed Res Int* **2018**, (2018).
44. Buchholz, H. W. & Engelbrecht, H. [Depot effects of various antibiotics mixed with Palacos resins]. *Der Chirurg; Zeitschrift für Alle Gebiete der Operativen Medizen* **41**, 511–515 (1970).
45. McConoughey, S. J., Howlin, R. P., Wiseman, J., Stoodley, P. & Calhoun, J. H. Comparing PMMA and calcium sulfate as carriers for the local delivery of antibiotics to infected surgical sites. *J Biomed Mater Res B Appl Biomater* **103**, 870–877 (2015).
46. Webb, J. C. J. & Spencer, R. F. The role of polymethylmethacrylate bone cement in modern orthopaedic surgery. *J Bone Joint Surg Br* **89**, 851–857 (2007).
47. Slane, J., Gietman, B. & Squire, M. Antibiotic elution from acrylic bone cement loaded with high doses of tobramycin and vancomycin. *J Orthop Res* **36**, 1078–1085 (2018).
48. Bishop, A. R., Kim, S., Squire, M. W., Rose, W. E. & Ploeg, H. L. Vancomycin elution, activity and impact on mechanical properties when added to orthopedic bone cement. *J Mech Behav Biomed Mater* **87**, 80–86 (2018).
49. Hinarejos, P. *et al.* Use of antibiotic-loaded cement in total knee arthroplasty. *World Journal of Orthopedics* **6**, 877 (2015).
50. Laycock, P. A. *et al.* In Vitro Efficacy of Antibiotics Released from Calcium Sulfate Bone Void Filler Beads. *Materials (Basel)* **11**, (2018).
51. Anagnostakos, K., Hitzler, P., Pape, D., Kohn, D. & Kelm, J. Persistence of bacterial growth on antibiotic-loaded beads: is it actually a problem? *Acta Orthop* **79**, 302–307 (2008).
52. Alt, V. Antimicrobial coated implants in trauma and orthopaedics-A clinical review and risk-benefit analysis. *Injury* **48**, 599–607 (2017).
53. Metsemakers, W. J., Moriarty, T. F., Nijs, S., Pape, H. C. & Richards, R. G. Influence of implant properties and local delivery systems on the outcome in operative fracture care. *Injury* **47**, 595–604 (2016).

54. Dunne, N. & Ormsby, R. W. MWCNT Used in Orthopaedic Bone Cements. *Carbon Nanotubes - Growth and Applications* (2011).
55. Kumar Bera, A. *et al.* Can Antibiotic-mixed Polymethyl Methacrylate-wrapped Intramedullary Nail be used for Post Nailing Infected Tibial Non-union as Definitive Treatment? *International Journal of Scientific Study* **122**, 122 (2017).
56. Athans, V., Veve, M. P. & Davis, S. L. Trowels and Tribulations: Review of Antimicrobial-Impregnated Bone Cements in Prosthetic Joint Surgery. *Pharmacotherapy* **37**, 1565–1577 (2017).
57. Ene, R., Nica, M., Ene, D., Cursaru, A. & Cirstoiu, C. Review of calcium-sulphate-based ceramics and synthetic bone substitutes used for antibiotic delivery in PJI and osteomyelitis treatment. *EFORT Open Reviews* **6**, 297 (2021).
58. Bistolfi, A. *et al.* Antibiotic-Loaded Cement in Orthopedic Surgery: A Review. *ISRN Orthopedics* **2011**, 1–8 (2011).
59. Dusane, D. H. *et al.* Effects of loading concentration, blood and synovial fluid on antibiotic release and anti-biofilm activity of bone cement beads. *J Control Release* **248**, 24–32 (2017).
60. Howlin, R. P. *et al.* Antibiotic-loaded synthetic calcium sulfate beads for prevention of bacterial colonization and biofilm formation in periprosthetic infections. *Antimicrob Agents Chemother* **59**, 111–120 (2015).
61. Oliver, R. A. *et al.* Development of a Novel Model for the Assessment of Dead-Space Management in Soft Tissue. *PLOS ONE* **10**, e0136514 (2015).
62. Cloutier, M., Mantovani, D. & Rosei, F. Antibacterial Coatings: Challenges, Perspectives, and Opportunities. *Trends Biotechnol* **33**, 637–652 (2015).
63. Arbade, G. K., Dongardive, V., Rath, S. K., Tripathi, V. & Patro, T. U. Effect of poly(ethylene glycol) on drug delivery, antibacterial, biocompatible, physico-chemical and thermo-mechanical properties of PCL-chloramphenicol electrospun nanofiber scaffolds. *Int. J. Polym. Mater. Polym. Biomater.* **71**, 208–219 (2020).
64. Chirife, J. *et al.* In vitro antibacterial activity of concentrated polyethylene glycol 400 solutions. *Antimicrobial Agents and Chemotherapy* **24**, 409 (1983).
65. Harris, L. G., Tosatti, S., Wieland, M., Textor, M. & Richards, R. G. Staphylococcus aureus adhesion to titanium oxide surfaces coated with non-functionalized and peptide-functionalized poly(L-lysine)-grafted- poly(ethylene glycol) copolymers. *Biomaterials* **25**, 4135–4148 (2004).

66. Balaure, P. C. & Grumezescu, A. M. Recent Advances in Surface Nanoengineering for Biofilm Prevention and Control. Part I: Molecular Basis of Biofilm Recalcitrance. Passive Anti-Biofouling Nanocoatings. *Nanomaterials* 2020, Vol. 10, Page 1230 **10**, 1230 (2020).
67. Zheng, S. *et al.* Implication of Surface Properties, Bacterial Motility, and Hydrodynamic Conditions on Bacterial Surface Sensing and Their Initial Adhesion. *Frontiers in Bioengineering and Biotechnology* **9**, 82 (2021).
68. Sim, W., Barnard, R. T., Blaskovich, M. A. T. & Ziora, Z. M. Antimicrobial Silver in Medicinal and Consumer Applications: A Patent Review of the Past Decade (2007–2017). *Antibiotics* **7**, (2018).
69. Bai, X., Sandukas, S., Appleford, M., Ong, J. L. & Rabiei, A. Antibacterial effect and cytotoxicity of Ag-doped functionally graded hydroxyapatite coatings. *J Biomed Mater Res B Appl Biomater* **100**, 553–561 (2012).
70. You, J., Zhang, Y. & Hu, Z. Bacteria and bacteriophage inactivation by silver and zinc oxide nanoparticles. *Colloids Surf B Biointerfaces* **85**, 161–167 (2011).
71. Park, H. J. *et al.* Silver-ion-mediated reactive oxygen species generation affecting bactericidal activity. *Water Res* **43**, 1027–1032 (2009).
72. Lepelletier, D., Maillard, J. Y., Pozzetto, B. & Simon, A. Povidone Iodine: Properties, Mechanisms of Action, and Role in Infection Control and Staphylococcus aureus Decolonization. *Antimicrob Agents Chemother* **64**, (2020).
73. Zhang, H. *et al.* Vancomycin-loaded titanium coatings with an interconnected micro-patterned structure for prophylaxis of infections: an in vivo study. *RSC Advances* **8**, 9223–9231 (2018).
74. Zhang, L. *et al.* Electrospun vancomycin-loaded coating on titanium implants for the prevention of implant-associated infections. *Int J Nanomedicine* **9**, 3027–3036 (2014).
75. Stevanović, M. *et al.* Assessing the bioactivity of gentamicin-preloaded hydroxyapatite/Chitosan composite coating on titanium substrate. *ACS Omega* **5**, 15433–15445 (2020).
76. Delcour, A. H. Outer Membrane Permeability and Antibiotic Resistance. *Biochim Biophys Acta* **1794**, 808 (2009).
77. Jiao, Y. *et al.* Quaternary ammonium-based biomedical materials: State-of-the-art, toxicological aspects and antimicrobial resistance. *Progress in Polymer Science* **71**, 53 (2017).

78. Asri, L. A. T. W. *et al.* A Shape-Adaptive, Antibacterial-Coating of Immobilized Quaternary-Ammonium Compounds Tethered on Hyperbranched Polyurea and its Mechanism of Action. *Advanced Functional Materials* **24**, 346–355 (2014).
79. Zhang, Y. *et al.* Gemini quaternary ammonium salt waterborne biodegradable polyurethanes with antibacterial and biocompatible properties. *Materials Chemistry Frontiers* **1**, 361–368 (2017).
80. Campoccia, D., Montanaro, L., Speziale, P. & Arciola, C. R. Antibiotic-loaded biomaterials and the risks for the spread of antibiotic resistance following their prophylactic and therapeutic clinical use. *Biomaterials* **31**, 6363–6377 (2010).
81. Pichavant, L. *et al.* pH-controlled delivery of gentamicin sulfate from orthopedic devices preventing nosocomial infections. *J Control Release* **162**, 373–381 (2012).
82. Zhang, Y. *et al.* Smart Titanium Coating Composed of Antibiotic Conjugated Peptides as an Infection-Responsive Antibacterial Agent. *Macromolecular Bioscience* **21**, 2000194 (2021).
83. Kurose, H., Miyagi, D., Takahashi, N., Uchida, N. & Kawanaka, K. 3-D Eddy current analysis of induction heating apparatus considering heat emission, heat conduction, and temperature dependence of magnetic characteristics. *IEEE Transactions on Magnetics* **45**, 1847–1850 (2009).
84. Pijls, B. G., Sanders, I. M. J. G., Kuijper, E. J. & Nelissen, R. G. H. H. Segmental induction heating of orthopaedic metal implants. *Bone Joint Res* **7**, 609–619 (2018).
85. Lucia, O., Maussion, P., Dede, E. J. & Burdio, J. M. Induction heating technology and its applications: Past developments, current technology, and future challenges. *IEEE Transactions on Industrial Electronics* **61**, 2509–2520 (2014).
86. Kok, H. P. *et al.* Heating technology for malignant tumors: a review. *Int J Hyperthermia* **37**, 711 (2020).
87. Giustini, A. J. *et al.* MAGNETIC NANOPARTICLE HYPERTHERMIA IN CANCER TREATMENT. *Nano Life* **1**, 17–32 (2010).
88. Liu, X. *et al.* Comprehensive understanding of magnetic hyperthermia for improving antitumor therapeutic efficacy. *Theranostics* **10**, 3793 (2020).
89. Kumar, C. S. S. R. & Mohammad, F. Magnetic Nanomaterials for Hyperthermia-based Therapy and Controlled Drug Delivery. *Adv Drug Deliv Rev* **63**, 789 (2011).
90. Tong, S., Zhu, H. & Bao, G. Magnetic Iron Oxide Nanoparticles for Disease Detection and Therapy. *Mater Today (Kidlington)* **31**, 86 (2019).

91. Zuvin, M. *et al.* Nanoparticle based induction heating at low magnitudes of magnetic field strengths for breast cancer therapy. *JMMM* **483**, 169–177 (2019).
92. Catalano, E. Targeted tumor drug delivery and magnetic hyperthermia for cancer treatment by chemotherapeutic-conjugated magnetic nanoparticles. *AIP Conference Proceedings* **1990**, 020022 (2018).
93. Ha, P. T. *et al.* Doxorubicin release by magnetic inductive heating and in vivo hyperthermia-chemotherapy combined cancer treatment of multifunctional magnetic nanoparticles. *New Journal of Chemistry* **43**, 5404–5413 (2019).
94. Fernandes, S. *et al.* Magnetic Nanoparticle-Based Hyperthermia Mediates Drug Delivery and Impairs the Tumorigenic Capacity of Quiescent Colorectal Cancer Stem Cells. *ACS Applied Materials and Interfaces* **13**, 15959–15972 (2021).
95. Pijls, B. G., Sanders, I. M. J. G., Kuijper, E. J. & Nelissen, R. G. H. H. Non-contact electromagnetic induction heating for eradicating bacteria and yeasts on biomaterials and possible relevance to orthopaedic implant infections: In vitro findings. *Bone Joint Res* **6**, 323–330 (2017).
96. Ricker, E. B. & Nuxoll, E. Synergistic effects of heat and antibiotics on *Pseudomonas aeruginosa* biofilms. *Biofouling* **33**, 855–866 (2017).
97. Müller, C. W. *et al.* Transcutaneous electromagnetic induction heating of an intramedullary nickel-titanium shape memory implant. *Int Orthop* **38**, 2551–2557 (2014).
98. Chopra, R. *et al.* Employing high-frequency alternating magnetic fields for the non-invasive treatment of prosthetic joint infections. *Sci Rep* **7**, (2017).
99. Tsitlanadze, G., Kviria, T., Katsarava, R. & Chu, C. C. In vitro enzymatic biodegradation of amino acid based poly(ester amide)s biomaterials. *J Mater Sci Mater Med* **15**, 185–190 (2004).
100. Winnacker, M. & Rieger, B. Poly(ester amide)s: recent insights into synthesis, stability and biomedical applications. *Polymer Chemistry* **7**, 7039–7046 (2016).
101. Zhang, S. *et al.* Poly(ester amide)-based hybrid hydrogels for efficient transdermal insulin delivery. *Journal of Materials Chemistry B* **6**, 6723–6730 (2018).
102. Ghosal, K., Latha, M. S. & Thomas, S. Poly(ester amides) (PEAs) – Scaffold for tissue engineering applications. *European Polymer Journal* **60**, 58–68 (2014).
103. Knight, D. K., Gillies, E. R. & Mequanint, K. Strategies in functional poly(ester amide) syntheses to study human coronary artery smooth muscle cell interactions. *Biomacromolecules* **12**, 2475–2487 (2011).

104. Villamagna, I. J., Gordon, T. N., Hurtig, M. B., Beier, F. & Gillies, E. R. Poly(ester amide) particles for controlled delivery of celecoxib. *J Biomed Mater Res A* **107**, 1235–1243 (2019).
105. Peters, T. *et al.* Evaluation of poly(esteramide) (PEA) and polyester (PLGA) microspheres as intravitreal drug delivery systems in albino rats. *Biomaterials* **124**, 157–168 (2017).
106. Qian, Z. *et al.* Glass Transition Phenomenon for Conjugated Polymers. *Macromolecular Chemistry and Physics* **220**, 1900062 (2019).
107. Soleimani, A., Drappel, S., Carlini, R., Goredema, A. & Gillies, E. R. Structure-property relationships for a series of poly(ester amide)s containing amino acids. *Industrial and Engineering Chemistry Research* **53**, 1452–1460 (2014).
108. Lips, P. A. M. *et al.* Biocompatibility and degradation of aliphatic segmented poly(ester amide)s: in vitro and in vivo evaluation. *J Biomed Mater Res A* **76**, 699–710 (2006).
109. Rodriguez-Galan, A., Franco, L. & Puiggali, J. Degradable Poly(ester amide)s for Biomedical Applications. *Polymers 2011, Vol. 3, Pages 65-99* **3**, 65–99 (2010).
110. Kropp, M. *et al.* Biocompatibility of Poly(ester amide) (PEA) Microfibrils in Ocular Tissues. *Polymers 2014, Vol. 6, Pages 243-260* **6**, 243–260 (2014).
111. Janssen, M. *et al.* Celecoxib-loaded PEA microspheres as an auto regulatory drug-delivery system after intra-articular injection. *J Control Release* **244**, 30–40 (2016).

Chapter 2

2 Thermo-responsive antibiotic-eluting coatings for treating infection near orthopedic implants

2.1 Introduction

Infection in the orthopedic field has become one of the major complications associated with orthopedic implants (hip, knee, and shoulder replacement) and trauma-related devices (nails, plates, and screws).^{1,2} Orthopedic infection can occur through various mechanisms such as hospital-acquired infections, bacterial contamination of the surgical site, or bacteria entering the surgical site from other locations of the patient's body.^{3,4} It is often associated with the metal surfaces of joint replacement or fracture fixation devices such as implants or plates, which are recognized by the body as foreign in which case it is referred to as orthopedic device-related infections (ODRI).⁵ Unfortunately, infections associated with joint replacement surgeries are growing with an estimated 2.7% of all surgeries performed resulting in infection.⁶ Upon diagnosis of an ODRI, the current standard of treatment is revision surgery.⁵ Despite its high reported success, there is a large and growing economic burden on the healthcare system coupled with a poorer quality of life for patients recovering from revision surgery.^{1,2,7,8} In the US, healthcare expenditures related to hip and knee revision surgeries are projected to reach \$1.85 billion (USD) by 2030 and on average, patients undergoing revision surgery require a longer hospitalized recovery time of approximately nine days as compared to only 3.8 days after primary surgery.^{3,7,8}

The main cause of ODRI is the initial interaction of planktonic bacteria with the surfaces of metal substrates known as reversible adherence. After some time, bacteria can fix themselves onto these surfaces and undergo irreversible attachment which initiates biofilm development.⁹ Fully matured biofilms are very complex structures, act as a barrier to the host's immune system, and can become very thick and difficult to remove if left untreated.¹⁰ As a result, there are limited clinical options for the treatment of ODRI besides revision surgery.^{11,12} For example, systemic antibiotic therapy can be used as a treatment but is often used alongside revision surgery and never stand-alone. Due to the

structure of the biofilm, antibiotics are unable to penetrate let alone eradicate an established mature biofilm and may potentially induce antibiotic-resistant bacteria. It would also require antibiotic concentrations that far exceed patients' toxic threshold.^{13,14} To enhance the efficacy of revision surgery to treat ODRI, systemic and local antibiotic therapies are often used. While intravenous or oral delivery of antibiotics suffers from the limitations described above, another approach has been to incorporate antibiotics into poly(methyl methacrylate) (PMMA) bone cement-based spacers as part of the two-stage revision surgery procedure.^{11,15,16} However, PMMA bone cement is not biodegradable, and many studies have reported that the eluted antibiotic concentrations are effective only in the first few postoperative hours, followed by the release of sub-inhibitory antibiotic concentrations for several days thereafter.¹⁷⁻²² A substantial portion of the drug is never released. Furthermore, the antibiotics must retain their chemical stability during the high local temperatures generated during the curing of bone cement, so only selected antibiotics such as vancomycin and gentamicin can be used.²³ These limitations have caused a shift towards the clinical use of resorbable materials such as calcium sulfate and calcium phosphate beads as antibiotic carriers. These carriers can release their antibiotic load more rapidly and completely and can be used with a wider range of antibiotics.^{19,24} However, several studies have reported instances where drug release from these carriers may be too fast.^{18,25} Other studies have reported varying antibiotic elution kinetics dependent on the amount of antibiotic-loaded into these carriers, which can affect the rate of degradation and antibiotic concentration levels over the short and long term.^{19,24,26,27} Thus, new delivery systems with prolonged and ideally controlled release of antibiotics are needed to treat ODRI.

Another approach that has been explored to prevent the growth of bacteria on a wide range of surfaces is the development of antibacterial or antibiotic-eluting coatings. Antibacterial coatings can work either passively by reducing bacterial adhesion or actively by releasing antibacterial agents that kill bacteria near the surface of the material.²⁸ For example, the use of chitosan has been explored for antibacterial coatings due to its antimicrobial properties, low toxicity, and the fact that it is well tolerated *in vivo*.²⁹ Chitosan possesses strong antibacterial activity because it can disrupt bacterial cell walls through electrostatic interactions between its polycationic structure and the anionic

structures of the bacterial cell wall. Chitosan has also been conjugated with antibacterial compounds such as enzymes (lysozyme and proteases), antibiotics (rifampicin and tobramycin), and metals to enhance its antibacterial properties on surfaces.³⁰ Cationic antibacterial quaternary ammonium compounds (QACs) have also been extensively investigated for the development of antibacterial surfaces. They also act through electrostatic interactions with bacteria, resulting in membrane disruption and the leakage of cytoplasmic material of bacteria.^{31,32} Furthermore, silver (Ag) has also been extensively investigated as an antibacterial agent in coatings for both consumer products and medical applications.^{33,34} Ag-based coatings work by several mechanisms. Ag cations can penetrate the bacterial cell wall and form reactive oxygen species that disrupt bacterial metabolic pathways, DNA replication, and cellular respiration.³⁵ Ag nanoparticles have been explored for implanted devices where the particles have been immobilized onto the surfaces of the devices by blending them with polymers to form composite coatings.^{36,37} However, there are still concerns about toxicity with silver-based nanoparticle coatings. Smaller Ag nanoparticles associated with orthopedic devices may be taken up by mammalian cells and there have been reports of cytotoxicity of Ag ions against osteoblasts and osteoclasts.^{35,38} Therefore, further research is required to evaluate the effects of circulating Ag nanoparticles *in vivo* and the controlled release of nanoparticles from coatings over the short and long term.³⁸ To address the limitations of current materials, researchers are now shifting to develop smart degradable coatings and nanoparticles that can be triggered to release drugs on demand or upon a change in the local environment that are associated with infection, such as changes in pH, bacterial by-products, or elevated temperature, yet ODRI remains a challenge.³⁹

Inspired by the use of induction heating (IH) in the field of cancer therapy, researchers have begun to explore the potential for IH to treat ODRI through the killing of planktonic bacteria and the disruption of biofilms.⁴⁰⁻⁴³ IH involves the use of a high frequency alternating magnetic field (AMF), to generate an electric current (eddy current) within a conductive material such as Ti or steel.⁴⁴ The flow of the eddy current through the resistance of the material results in rapid Joule heating without any external heat source or contact with the heating device and with minimal heating of surrounding tissues.^{42,45} In the orthopedic field, non-contact heating of metal substrates potentially allows for a non-

invasive approach to resolving ODRI. However, based on the reported studies, IH alone is unlikely to be sufficient to completely eradicate an infection even at high temperatures ranging from 80 – 90 °C.^{41,43,45,46} The main limitations of IH that relate to the orthopedic field have been tissue necrosis, the high power and length of IH exposure, and the heating uniformity of objects with complex shapes. In particular, the viability of the tissue layer that is nearest to the surface of the metallic device that is being heated is a concern, although several studies have suggested that tissues can recover post-heating.⁴⁷ Intermittent heating can also potentially be used to minimize tissue necrosis.⁴⁵ Furthermore, studies have suggested that IH may enhance the sensitivity of bacteria to antibiotics,^{43,46–48} providing a potential avenue to reduce the time and intensity of thermal treatment while enhancing bacterial killing.

Described here is a new approach using IH to directly kill bacteria and inhibit biofilm formation and achieve on-demand externally triggered release of antibiotics (Figure 2.1). The design involves the use of a poly(ester amide) (PEA) coating with a glass transition temperature (T_g) of 39 °C. In addition to the ability to readily tune the properties of PEAs through the incorporation of specific monomers,^{49–51} they have been reported to be well tolerated *in vivo* with a wide range of biomedical applications including in hydrogel and particle-based drug delivery systems,^{52–54} scaffolds for tissue regeneration,^{55–57} and ocular implants.⁵⁸ It is demonstrated that in the absence of direct heating or IH, the PEA coating erodes and releases rifampicin over a period of > 100 days, whereas with heating above the PEAs T_g , this release can be greatly accelerated due to increased mobility of the drug in the PEA film in its rubbery state. Additionally, the use of an intermittent IH protocol achieves substantial rifampicin release within a one-hour heating cycle. Against *S. aureus*, IH and the thermally triggered release of rifampicin lead to synergistic reductions in biofilm formation and live bacteria on the surface.

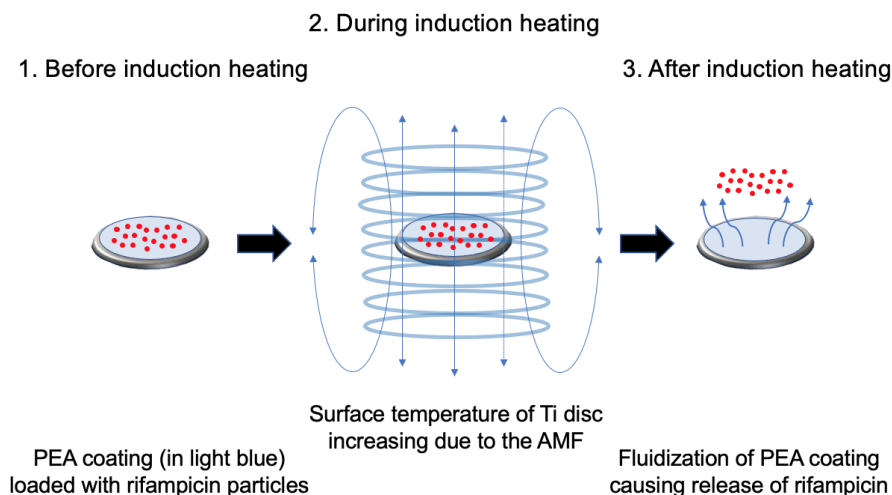


Figure 2.1: Schematic showing a thermo-responsive drug-eluting PEA coating triggered by IH using an alternating magnetic field. The heating of the PEA above its T_g results in increased drug mobility and the release of rifampicin from the surface.

2.2 Experimental

2.2.1 General experimental details

A PEA composed of phenylalanine, 1,4-butanediol, and sebacic acid (PBSe) and a control PEA composed of phenylalanine, butanediol, and terephthaloyl chloride (PBTe) were synthesized and characterized as previously reported (Figures A1-A3).^{51,55} The batch of PBSe polymer used had a number average molar mass (M_n) of 79 kg/mol, and a dispersity (D) of 2.5, while PBTe had an M_n of 18 kg/mol and D of 2.8. Rifampicin was purchased from Ontario Chemicals Inc. (Guelph, ON, Canada). Dimethyl sulfoxide (DMSO) (reagent grade), dichloromethane (DCM) (glass distilled), dimethylformamide (DMF) (glass distilled) and high-performance liquid chromatography (HPLC) grade acetonitrile (99.8%) were purchased from Caledon (Halton Hills, ON, Canada). Glacial acetic acid (reagent grade) was purchased from Caledon Laboratories Limited (Georgetown, ON, Canada). Phosphate-buffered saline (PBS) was made with deionized (DI) water from a MilliQ system, to create PBS, pH 7.4. Tryptic soy broth, D-(+)-glucose powder (bioreagent suitable for cell culture), chloramphenicol (Cm) (Bioreagent suitable for plant cell culture), and 3-(4,5-dimethylthiazol-2-yl)-2,5-diphenyl tetrazolium bromide

(MTT) was purchased from Millipore-Sigma (Oakville, ON) and were used as purchased without further purification. UV-visible spectroscopy was performed using a Varian Cary 300 UV-visible spectrophotometer purchased from Varian (Palo Alto, California, USA).

2.2.2 Coating preparation

In this study, polymer-antibiotic blends were prepared using weight percentages of 2.5, 5, and 10% (w/w) of rifampicin relative to the polymer. Rifampicin and the PEA were co-dissolved in DMF at a total concentration of 16.25 mg/mL (polymer + drug), with the ratios adjusted depending on the desired percentage of drug.

An aliquot of 500 μ L was drop-casted onto a 3D-printed Ti-6Al-4V alloy disc, 2 cm in diameter and 3 mm in thickness. After the solution was spread uniformly across the surface, the discs were dried in a vacuum oven at 50 °C overnight. The coating thickness was measured using a digital micrometer (Mitutoyo Digital Micrometer, H-2780, Japan) by calculating the difference between coated and non-coated 3D-printed Ti alloy discs. Pipetting 500 μ L of the 2.5% (w/w) stock solution onto Ti discs led to an 8.4 ± 1.3 μ m thick coating.

2.2.3 Thermal analysis of rifampicin-PEA blends

Rifampicin-PEA solutions in DMF were prepared as described in the coating preparation section. The solution was then dropped cast onto a glass petri dish and dried in a vacuum oven at 50 °C overnight resulting in a thin film. The films are then washed with deionized water and lyophilized. Thermal analysis was performed using a Q2000 Differential Scanning Calorimeter (DSC) (TA Instruments, New Castle, DE, USA). The heating/cooling rate was 10 °C/min from 0 to +200 °C, and the data was obtained from the second heating cycle.

2.2.4 Scanning electron microscope (SEM)

SEM was performed using a Zeiss LEO 1530 instrument, operating at 2.0 kV and a working distance of 6 mm. Dried coating samples were mounted onto stubs covered in carbon tape and coated with a 10 nm layer of osmium, using an SPI Supplies, OC-60A

plasma coater. Micrographs of the surface of the coatings were taken at different magnifications.

2.2.5 *In vitro* release of rifampicin

The coatings were prepared as described above. Each disc was suspended in 20 mL of PBS. To measure release in the absence of thermal triggering, the samples were incubated in an oven at 37 °C for 100 days with aliquots (3 mL) of the medium, taken daily for 20 days and then every 5 days to measure the release of rifampicin. On days 20, 50, and 75 all the media was replaced with fresh PBS.

To assess the effect of temperature on the rifampicin release rate, samples were also incubated in baths with set temperatures from 50 – 80 °C, in increments of 10 °C, for 3 h with 3 mL aliquots taken for measurement and with all the media replaced with fresh PBS every 30 min. The drug released was assessed in the PBS solution using UV-visible spectroscopy at a wavelength of 332 nm based on an extinction coefficient of 18123 L mol⁻¹ cm⁻¹ for rifampicin in the same buffer system. Each sample and condition was studied in triplicate and the results are presented as the mean ± standard deviation.

2.2.6 *In vitro* degradation of coating in PBS

Rifampicin-PEA coatings (5% w/w drug) were prepared by adding 10 mL of the PEA-rifampicin solution in DMF (30 mg/mL) to pre-weighed 5-dram vials and then drying the coatings overnight in a vacuum oven at 50 °C. To measure coating mass loss over time at physiological temperature, the samples were incubated in a 37 °C oven for 105 d. Every 15 d, triplicate samples were removed, PBS was discarded, and the coatings were washed using deionized water. They were then dried to constant mass in a vacuum oven at 37 °C and then weighed to determine mass loss.

To assess the effect of temperature on the degradation, the samples were incubated at set temperatures from 50 – 80 °C, in increments of 10 °C, for 3 h. Triplicate samples were removed every hour, washed, dried, and weighed as described above. The percent coating mass remaining was calculated as (mass at the measurement time/initial mass)*100%.

Each condition was evaluated in triplicate and the results are presented as the mean \pm standard deviation.

2.2.7 Induction heater design

A solenoid coil (40 mm ID and 10 cm in length) and a zero-voltage flyback transformer were developed to expose a Ti disc sample to a high-frequency alternating magnetic field (AMF) (Figure 2.2). An induction frequency of 123 kHz was transmitted through the coil controlled by an Arduino. To monitor the surface temperature of the Ti disc a 3D-printed mount was constructed to hold a K-type thermocouple positioned in contact directly against the surface of the Ti disc and co-axially aligned with the solenoid coil (Figure 2.3). The instantaneous power delivered to the induction heater unit was controlled in real-time by pulse-width modulation via a proportional-integral-derivative (PID) control loop. The parameters associated with the PID loop were optimized, ensuring that the desired temperature was reached within about 40 s, with minimal overshoot (± 0.5 °C). Additionally, a 3D-printed dish made from polyethylene terephthalate glycol (PETG) was used as a sample holder for the Ti disc that could be seated at the center of the solenoid coil below the thermocouple.

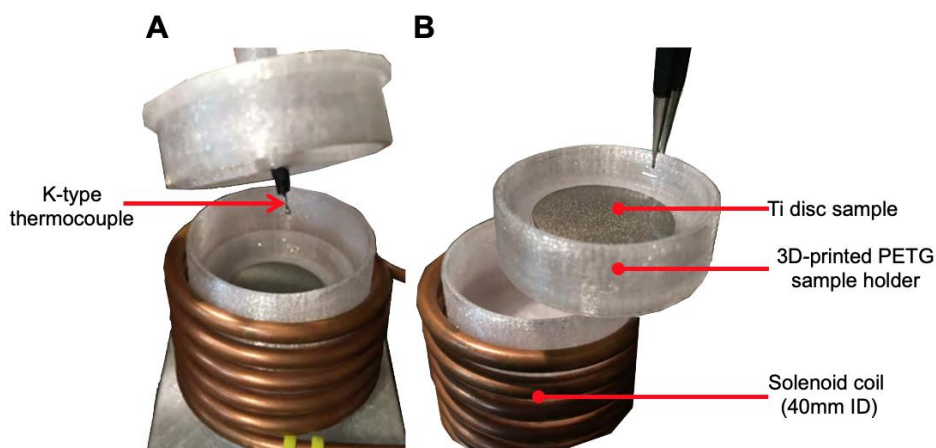


Figure 2.2: A) Frontal view of the induction device setup showing a solenoid coil (40 mm ID) wrapped around a 3D-printed PETG cylinder holding in place the PETG sample holder with the K-type thermocouple co-axially aligned with the Ti disc sample. B) The position of the Ti disc sample within the PETG sample holder.

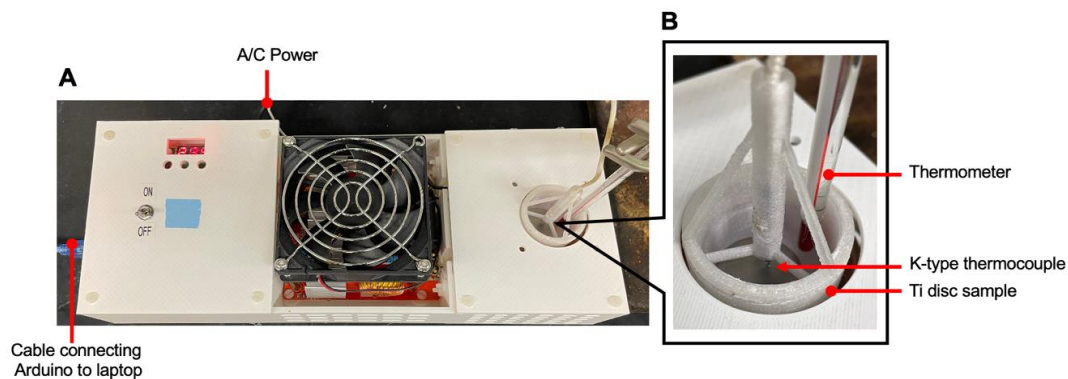


Figure 2.3: A) Top view of the custom-made inductive heating device and B) Exploded view of a 3D-printed Ti disc sample at the center of a PETG sample holder with a K-type thermocouple in contact with the surface of the Ti disc and thermometer to measure the surrounding medium temperature.

2.2.8 Rifampicin release triggered by induction heating

For all IH experiments, a PBSe-rifampicin blend of 2.5% (w/w) and a coating thickness of $8.4 \pm 1.3 \mu\text{m}$ was used. Coated discs were placed within the PETG sample holder and suspended in 5 mL of PBS with the K-type thermocouple positioned in direct contact with the sample's surface. Samples were exposed to an AMF with cycles of 6 min on and 6 min off over a period of one hour to evaluate the relationship between AMF exposure and drug release.

After various set time points, the PBS was collected for analysis and the sample was re-suspended with new fresh PBS. The solution was analyzed for rifampicin as described in the section on *in vitro* release of rifampicin. A set maximum temperature of $50 \text{ }^\circ\text{C}$ was used for all IH experiments as it allowed the surrounding medium not to exceed $40 \text{ }^\circ\text{C}$. This was validated using a thermometer that was placed in the media within the PETG sample holder adjacent to the sample (Figure 2.3). Samples were also exposed to a constant AMF at a control temperature of $37 \text{ }^\circ\text{C}$. During IH experiments, power and temperature control were monitored and recorded via Arduino software.

2.2.9 Fibrinogen adsorption

Fibrinogen from human plasma (50 – 70% protein) was purchased from Millipore-Sigma (Oakville, ON), aliquoted, and stored at -20 °C. Before coating, the aliquots were thawed, diluted to 25 µg/mL in 0.9% NaCl, and sterilized by filtration through a 0.22 µm low binding protein syringe filter. Ti discs were placed in six-well plates and coated with fibrinogen via immersion in 3 mL of the fibrinogen solution for 30 min incubating at 37 °C. Then, the discs were removed and dried at room temperature overnight in a glass petri dish.

2.2.10 Biofilm culture and growth conditions

S. aureus (ATCC 6538) was grown using a tryptic soy agar (TSA) plate incubated for 18 h at 37 °C, followed by the inoculation of a single colony in tryptic soy broth (TSB) for bacterial culture. The *S. aureus* was maintained over the long term in a glycerol stock incubated at -80 °C.

The sample groups included PBSe coatings without IH or rifampicin, PBSe coatings with IH and no rifampicin, rifampicin-loaded PBSe coatings and no IH, and rifampicin-loaded PBSe coatings with IH. Coatings were prepared by drop-casting 500 µL of a 2.5% (w/w) stock solution of rifampicin-PBSe with a coating thickness of 8.4 ± 1.3 µm. Biofilms were grown in TSB supplemented with 1% glucose. This media was inoculated with *S. aureus* using an inoculation loop and incubated for 24 h at 37 ± 0.5 °C. The inoculated media was diluted to a bacterial concentration of approximately 10^8 colony-forming units per mL (CFU/mL), validated with the optical density of the stock measured at 600 nm using a spectrophotometer. The stock was further diluted with sterile TSB + 1% glucose to give a working bacterial concentration of approximately 10^5 CFU/mL. Coated and uncoated Ti discs were sterilized using the biosafety cabinet UV light for 1 h on each side and then were immersed in 10 mL of the inoculated media for 2 h, allowing for bacterial adherence. Afterwards, the excess media was discarded, and discs were incubated in 10 mL of fresh media for 48 h at 37 °C.

2.2.11 Effect of different combinations of IH and antibiotics on *S. aureus* biofilm growth and the bacterial viability

Coated Ti discs were prepared via drop-casting 500 μL of a 2.5% (w/w) stock solution with a coating thickness of $8.4 \pm 1.3 \mu\text{m}$ and sterilized as described in the section on biofilm culture and growth conditions. *S. aureus* was cultured in TSB + 1% glucose and with sample surfaces immersed in the suspension as described in the same section. Immediately after the 2 h incubation period for bacterial adherence, discs were transferred to the PETG sample holder and immersed in 5 mL of fresh TSB and 1% glucose. Samples were then exposed to an AMF intermittently, 6 min on and off, for a total period of 60 min. A maximum set temperature of 50 °C was used to prevent the surrounding medium in the sample holder from exceeding 40 °C. Upon completion of intermittent AMF exposure, the discs and 5 mL of media were transferred into a new small polystyrene petri dish containing 5 mL of fresh media for an added total of 10 mL and then incubated for 24 h at 37 °C. After 24 h, the disc and 5 mL of media were again transferred to the PETG sample holder, the induction heating process was repeated as above, and then the disc and media were transferred back to the petri dish and incubated for an additional 24 h.

Biofilm formation was assessed using crystal violet (CV) staining.^{59,60} After the incubation period, excess media was removed, and the discs were gently rinsed in fresh PBS three times. The biofilms were fixed by incubation for 1 h at 60 °C and then stained by immersion of the discs in 5 mL of 0.1% CV for 2 h in a 6-well polystyrene plate. The excess stain solution was removed, and the samples were gently rinsed with sterile distilled water. The stained biofilms were then destained using 33% acetic acid and the optical density of the acetic acid solution was measured at 595 nm using a Tecan Infinite M1000 Pro plate reader using Costar 96-well UV plates (#3635) with UV transparent flat bottoms. Each treatment group was evaluated in triplicates with the results calculated into percent biofilm formation.

The viability of the *S. aureus* after the different treatments was also quantified. After the completion of each treatment, the Ti discs were placed in 50 mL centrifuge tubes and the established biofilms were disrupted using a Fisher Scientific Ultrasonic Bath FS20H

(Hampton, NH, USA) for 20 minutes at 40 kHz. The Ti discs were removed and then the sonicated suspension was centrifuged for 15 min at 5000 rpm in a VWR Clinical 200 Centrifuge (Radnor, PA, USA). The suspension was subsequently vortexed and then serially diluted 10-fold into 15 mL centrifuge tubes. 10 μ L of each dilution were spot plated onto TSA plates and allowed to absorb for 30 min. The TSA plates were then inverted and incubated at 37 °C for 24 h. The plates prepared from dilutions that resulted in 3 – 50 CFUs were counted and after taking dilutions into account the CFU reduction for each treatment was calculated. Each treatment was analyzed in triplicate and the mean \pm standard deviation is reported.

2.2.12 Fluorescence microscopy of GFP-labeled *S. aureus* on coated discs

To visualize the effects of rifampicin-PEA coatings with and without IH on *S. aureus* biofilms, green fluorescent protein (GFP) expressing *S. aureus* was used. The *S. aureus* (ACC 6538) strain was transformed by electroporation with the plasmid pCG44 to enable GFP expression.^{61,62} The plasmid was maintained in *S. aureus* by culture in the presence of Cm at a final concentration of 10 μ g/mL. TSB + 1% glucose + Cm were inoculated with the new GFP *S. aureus* for 24 h at 37 °C. The inoculated media was then diluted to a working bacterial concentration of approximately 10⁵ CFU/mL. Discs were then exposed to the same conditions as described in the induction heating conditions for biofilm studies. Upon completion, the discs were gently rinsed with PBS and taken for microscopy. Imaging was performed using a Nikon Eclipse Ti2E Inverted Deconvolution Microscope from Nikon Instruments Canada Inc (Mississauga, ON, Canada) at a magnification of 20X.

2.2.13 Live/dead analysis of *S. aureus* on coated discs

To visualize the viability of *S. aureus* biofilms, after a 48 h incubation period, a LIVE/DEAD BacLight Bacterial Viability Kit for microscopy (L7007) was purchased from Thermofisher Scientific (Waltham, MA, USA). Bacteria cells were stained with propidium iodide (PI) to detect dead cell populations of *S. aureus* and SYTO 9 to detect viable cells. The stain mix was prepared according to the manufacturer's instructions and

added directly onto the surfaces of all samples and incubated at room temperature for 10 min in the dark. Live controls were allowed to grow undisturbed for the 48 h period and dead controls were heat shocked at 150 °C for 10 min. All treatment samples are then observed under the same microscope and analyzed with the exposure time intensity set according to the live and dead controls.

2.2.14 Mammalian cell viability

RAW 264.7 (ATCC TIB-71TM) immortalized murine macrophages were cultured in Dulbecco's Modified Eagle Medium (DMEM) containing 10% fetal bovine serum (FBS) and supplemented with antibiotics penicillin and streptomycin, 100 units/mL each (Life Technologies, Burlington, Canada) at 37 °C in the presence of 5% CO₂. Cells were split using a tissue culture scraper according to the manufacturer's instructions when they reached ~75% confluence. Ti discs coated with only PBSe as described in the coating preparation section and uncoated Ti discs were sterilized by irradiation using a biosafety cabinet UV light for 1 h on each side.

Cells were then seeded at a density of 184,000 cells (300 µL) onto each Ti disc in a six-well polystyrene plate and incubated for 3 h to allow initial adherence. An additional 3 mL of culture media is added to each well and samples were incubated for 24 h. Wells of the six-well polystyrene plate was used as a positive control and culture media alone was used as a negative control. After 24 h, PBSe-coated Ti discs were subjected to a 1 h IH protocol (alternating 6 min on, 6 min off at a set maximum temperature of 50 °C). Upon completion of the IH cycle, the medium was aspirated and replaced with 3 mL of 0.5 mg/mL of MTT in the culture media and the cells were incubated for 3 h. The MTT solution was then carefully aspirated, and 1 mL of DMSO was added to each well to solubilize the purple crystals. The absorbance of each well at 570 nm was then read in a plate reader (Tecan Infinite M1000 Pro) to quantify the relative metabolic activities of the RAW macrophages. Triplicates of all treatments were performed, and the results presented as the mean \pm standard deviation.

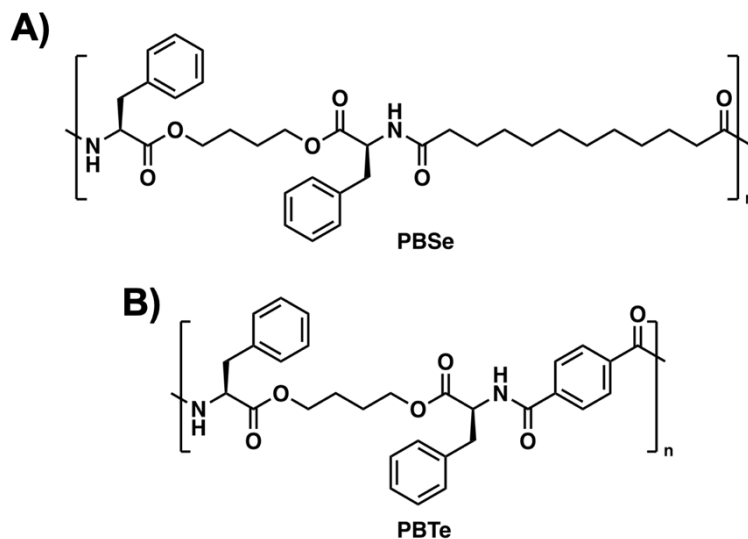
2.2.15 Statistical analysis

Quantitative differences between sample groups were reported as the mean \pm standard deviation (SD), and statistical analyses were performed using a one-way ANOVA with a Tukey's post-hoc test (Figure 2.10 & 2.13). Differences were considered statistically significant at $p < 0.05$.

2.3 Results and discussion

2.3.1 Preparation and characterization of PEA coatings

As a PEA with a thermal transition just above physiological temperature, PBSe composed of L-phenylalanine, 1,4-butanediol, and sebacic acid was selected (Scheme 2.1A). It has previously been reported to have a Tg of about 40 °C. As a control polymer to evaluate the effect of heating without passing through a glass transition, PBTe was chosen.⁵⁴ This PEA, composed of L-phenylalanine, 1,4-butanediol, and terephthalic acid (Scheme 2.1B), has been reported to have a Tg of about 100 °C.⁵¹ PBSe and PBTe were prepared as previously reported.^{51,55} To prepare the PEA-rifampicin blend coatings, DMF was used as it is a common solvent for the PEA and rifampicin. Drop-casting was employed, involving deposition of the polymer-drug solution onto the surface of a 3D-printed Ti-6Al-4V alloy disc, that had been sterilized using ethanol, followed by incubation overnight in a vacuum oven at 50 °C. The resulting polymer-drug layer on the Ti surface was attached via mechanical adhesion after solvent evaporation where the coating had anchored itself into the pores and depressions of the 3D-printed Ti-6Al-4V alloy disc. With a stock solution of 2.5% (w/w drug) a film thickness of $8.4 \pm 1.3 \mu\text{m}$ is obtained and can be tailored depending on the desired percentage of drug or polymer.



Scheme 2.1: Chemical structure of A) PBSe and B) PBTe.

The thermal properties of the rifampicin-PEA blend coatings were evaluated by DSC and were found to vary within a few degrees after incorporation of the drug. While PBSe had a T_g of 39 °C, the incorporation of 2.5, 5 and 10% (w/w) of rifampicin relative to polymer resulted in small increases in T_g to 41, 43, and 45 °C, respectively (Figure 2.4). The incorporation of 5 and 10% (w/w) of rifampicin into PBTe resulted in an increase in T_g from 95 °C for the pure polymer to 97 °C and 98 °C for 5 and 10% rifampicin. Rifampicin alone did not show any sign of a melting point or glass transition below 200 °C as indicated by the DSC curve, however, it is reported that the melting point of crystalline rifampicin is in the approximate range of 185-195 °C (Figure A4).⁶³

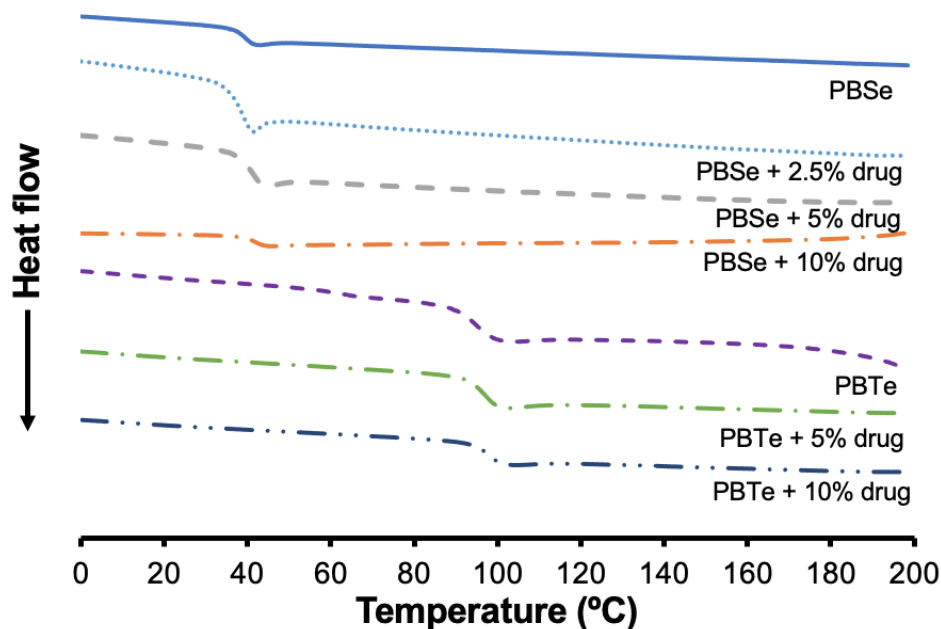


Figure 2.4: DSC thermographs of pure PBSe and PBTe and their formulations with rifampicin. The incorporation of antibiotic led to modest increases in the T_g .

2.3.2 *In vitro* release of rifampicin in the absence of the thermal triggering

First, the release of rifampicin at a physiological temperature of 37 °C from PEA coatings on Ti discs was studied (Figure 2.5). Each of the 2.5, 5 and 10% (w/w) rifampicin-PBSe coatings underwent an initial burst release, ranging from around 5% for the 2.5% coatings to almost 30% for the 10% coating, within the first 5 days. This initial release likely corresponded to the drug that was at or near the surface and therefore could be released without substantial PEA degradation. This initial release was followed by a slower release of rifampicin, with about 17% of rifampicin released from the 2.5% coating and 53% released from the 10% coating over 100 days (Figure 2.5). These results indicate that sustained release of rifampicin from PEA coatings can be achieved, providing a depot of remaining drug that can potentially be triggered for release for multiple months after implantation.

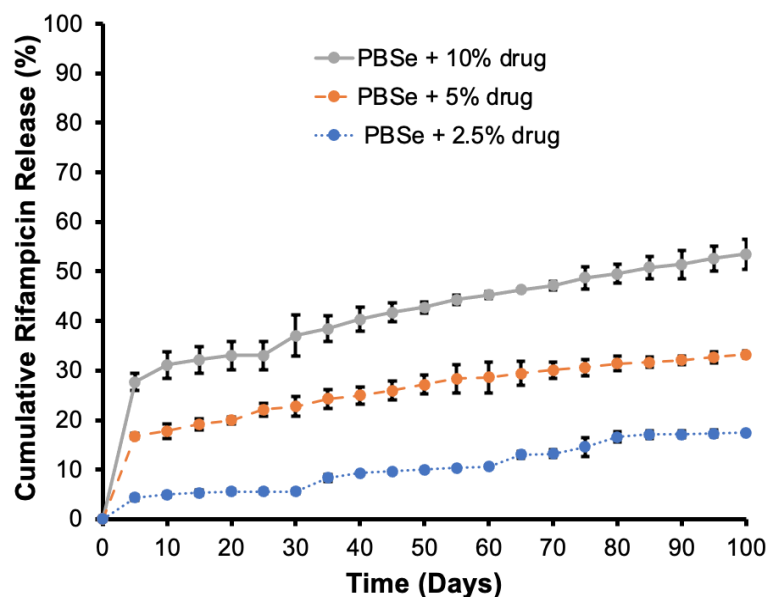


Figure 2.5: Release of rifampicin from PEA containing A) 5% (w/w) and B) 10% (w/w) drug on Ti discs suspended in PBS at varying temperatures. More rapid release of drug occurred for the PBSe coatings but not for the PBTe coatings at elevated temperatures. Error bars correspond to the standard deviations on triplicate samples.

The slow degradation of the PBSe coatings was also demonstrated by mass loss and SEM for 5% (w/w) rifampicin coatings incubated at 37 °C for more than 100 days. A 15% reduction in coating mass was observed over 15 days (Figure 2.6A). During the next 90 days, only a further 5% mass loss occurred, confirming the slow degradation of PBSe. SEM of PBSe-rifampicin coatings, before incubation, showed that the surface of the coating was smooth and quite homogenous (Figure 2.7A). After 60 days, the surface became rougher, suggesting that some erosion of the polymer surface had occurred (Figure 2.7B). After 105 days, substantial erosion of the surface was observed (Figure 2.7C). Samples incubated at 80 °C for three hours showed no visible surface degradation of the PBSe coating, however, many holes covered the coating's surface and can be recognized as the location of rifampicin being released before heating (Figure 2.7D).

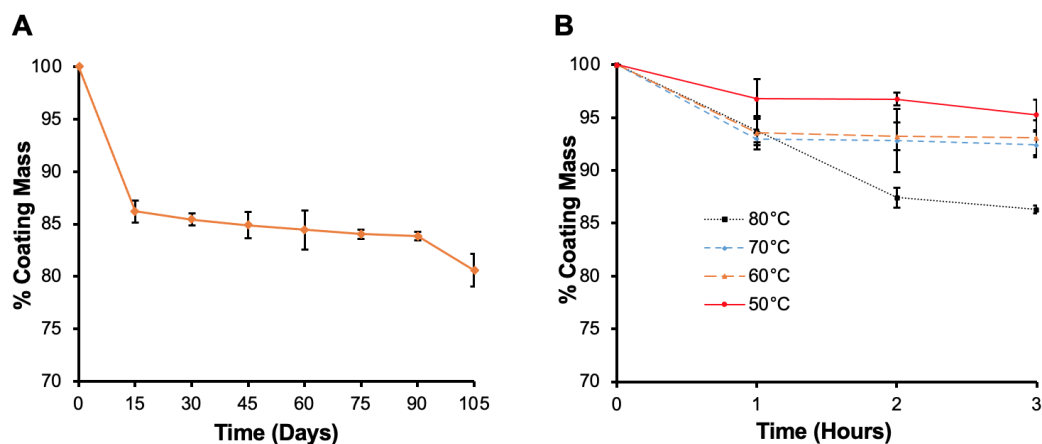


Figure 2.6: Degradation, based on mass loss, of PBSe coatings containing 5% (w/w) of rifampicin incubated in PBS at A) 37 °C for 105 days or B) temperatures ranging from 50 – 80 °C for 3 h. The coatings remained largely intact with minimal mass loss during each of these experiments. Error bars correspond to the standard deviations on triplicate samples.

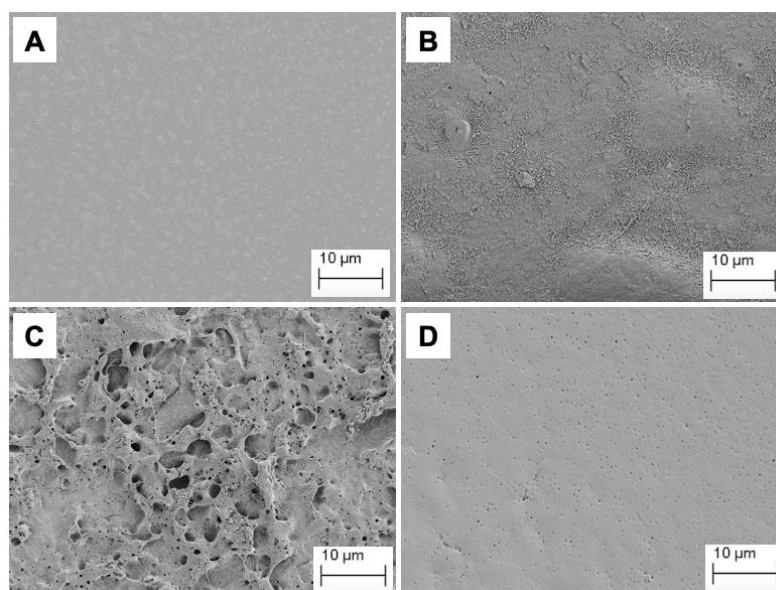


Figure 2.7: Scanning electron micrographs of the surface of PBSe-rifampicin coatings (5% (w/w) drug) A) Prior to incubation; B) After incubation at 37 °C for 60 days; C) After incubation at 37 °C for 105 days; D) After incubation at 80 °C for 3h.

2.3.3 Thermally triggered rifampicin release

Next, the ability to trigger the accelerated release of rifampicin above the T_g of the PEA was demonstrated. The rifampicin-PEA coatings were incubated in PBS at temperatures from 50 - 80 °C. At 80 °C, more than 70% of rifampicin was released from the 5% coating (Figure 2.8A) while almost 90% of the rifampicin was released from the 10% (w/w) rifampicin coating within 3 h (Figure 2.8B). Even at 60 °C, more than 30% of the rifampicin was released from both the 5 and 10% coatings, with the release slower at 50 °C. Most physicochemical processes, including drug release, are expected to be faster at higher temperatures. Therefore, to demonstrate that the accelerated release of rifampicin from the PBSe coatings was indeed due to the T_g of the polymer, the release rates of rifampicin from the control PBTe coatings with T_g values of ~100 °C were also evaluated at 50 – 80 °C. At each temperature, 10% or less of the loaded rifampicin was released from these coatings, thereby demonstrating the important role of the PBSe glass transition in facilitating drug release. Furthermore, to confirm that the accelerated drug release from the PBSe coatings at elevated temperatures was not simply a result of accelerated PEA degradation, mass loss from the coatings was examined. The mass loss ranged from 5 – 14% over 3 h from 50 – 80 °C (Figure 2.6B). Compared to 37 °C over 100 days, there was more drug release but less mass loss from the PBSe coatings at 50 – 80 °C over 3 h, confirming that the drug release was not rate-limited by polymer degradation at the elevated temperatures. Furthermore, SEM micrographs of the surface of PBSe-rifampicin coatings incubated at 80 °C for 3 h showed minimal polymer degradation but small pores were present, possibly due to loss of the drug from these areas of the surface (Figure 2.7D).

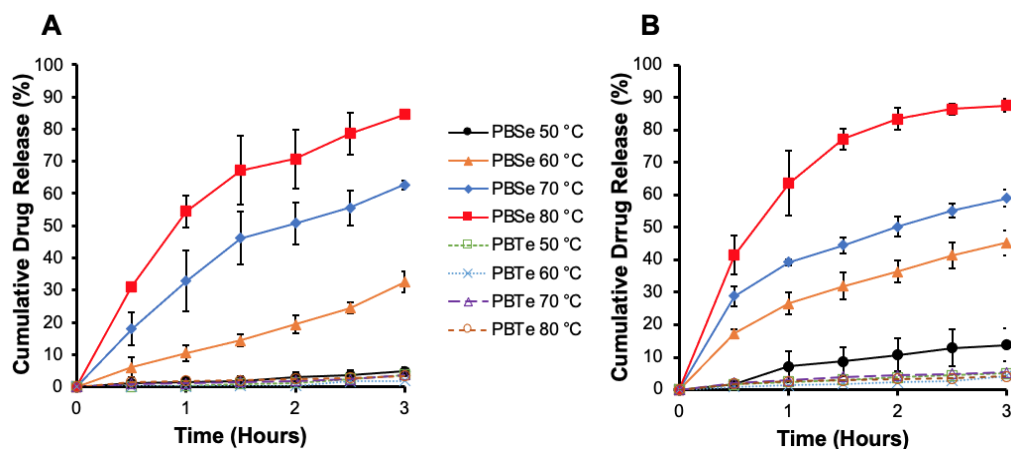


Figure 2.8: Release of rifampicin from PEA coatings containing A) 5% (w/w) and B) 10% (w/w) drug on Ti discs suspended in PBS at varying temperatures. More rapid release of drug occurred for the PBSe coatings but not for the PBTe coatings at elevated temperatures. Error bars correspond to the standard deviations on triplicate samples.

Overall, the results support that the acceleration in rifampicin release can be attributed to heating the coating above the T_g of PBSe. As the temperature of the PBSe coating is raised, the polymer chains become mobile, allowing the drug to diffuse through the coating to the surface, where it can then dissolve into solution. On the other hand, PBTe coatings remained below the polymer's T_g , where the polymer chains are rigid.

2.3.4 Drug release induced by IH

A custom-made inductive heating device was developed that allowed a Ti disc to be placed in a PETG sample holder such that the disc is positioned at the center of a solenoid coil (Figure 2.3). The sample holder could be filled with 5 mL of media and the temperature of the disc and media were monitored separately using a K-type thermocouple and a thermometer, respectively (Figure 2.2). Different IH protocols were considered with the aim of triggering rifampicin release while minimizing potential damage to surrounding cells and tissues. Studies have shown that the use of continuous AMF or highly hyperthermic conditions can cause necrosis of tissue, fat, or bone that surrounds the surface of the metal substrate.⁶⁴⁻⁶⁶ However, using an intermittent AMF has

been shown to generally overcome this limitation depending on the induction frequency and power. For example, Chopra and colleagues concluded that their *in vivo* results using intermittent heating of a metal ball implanted in the dorsal thigh muscle of a mouse model at 190 W for 220 seconds and 800 W for 15 seconds reaching temperatures of around 60 °C resulted in minimal thermal damage to muscle fibers, connective tissue, and vascular channels localized to less than 2 mm around the implants.⁴³ High thermal doses are very common in orthopedic surgery during processes such as drilling and cement fixation.^{45,67,68} While studies have shown that temperatures ranging from 60 – 80 °C result in tissue necrosis, the same studies also report on the ability of tissue recovery post-heating.^{43,45,47,69,70} Müller et al. reported that temperatures of 40 – 60 °C achieved via IH of an intramedullary nickel-titanium implant resulted in no signs of bone or tissue necrosis that surrounded the implant.⁴⁵ Based on these studies, we decided to limit the surface temperature of the Ti disc to 50 °C. We found that it was possible to perform five cycles (6 min on, 6 min off) or six cycles (5 min on, 5 min off) up to 50 °C over a period of 1 h without the surrounding bath temperature exceeding 40 °C, showing that it was possible to achieve selective heating at the metal surface while minimizing potential impacts on surrounding cells and tissues. After each heating cycle, the discs remained at 50 °C for 1-2 min, and then slowly decreased in temperature reaching around 45 °C after 3 min.

As designed, cycles of IH leading to heating of the coating above the polymer T_g accelerated drug release. PBSe coatings ($8.4 \pm 1.3 \mu\text{m}$ thickness) containing 2.5% (w/w) rifampicin released only 8% of the drug at the end of 60 min over a constant AMF at a set temperature of 37 °C. On the other hand, five cycles of intermittent IH with a set limit of 50 °C (6 min on, 6 min off) led to 26% rifampicin release over 60 min. Six shorter intermittent cycles at 50 °C (5 min on, 5 min off) resulted in a slower release of rifampicin with 21% released in 60 min (Figure 2.9). It appears that extending the duration of AMF can increase the release of rifampicin. However, the more rapid release of rifampicin in a shorter amount of time from these coatings compared to those studies in the direct heating experiment (Figure 2.8) can likely be attributed to thickness, as it may be easier for the drug to diffuse to the surface of the coating in a thinner coating. As

for the drug release experiments performed with direct heating of the solution, the mechanism of accelerated drug release is proposed to involve the heating of PBSe above its T_g , facilitating the diffusion of the drug to the coating surface, where it can be released. However, the key advantages of IH are that it can be performed remotely, using only an alternating magnetic field and that the heating can be applied selectively to the metals surface, allowing temperatures well above physiological temperature to be achieved at the site of the coating (e.g., 50 °C), while maintaining the temperature of the surroundings close to normal physiological temperature.

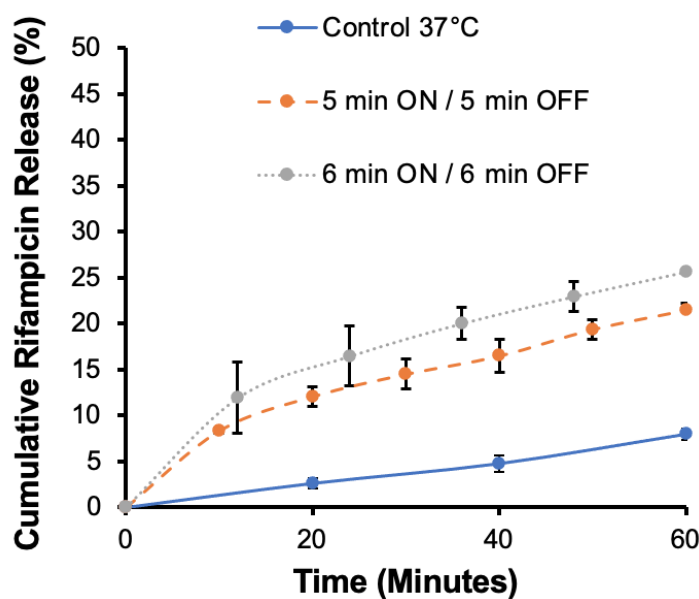


Figure 2.9: Release of rifampicin from inductively heated PBSe coatings on Ti discs using two different heat cycling procedures and compared to the same coatings without inductive heating, held at 37 °C. Error bars correspond to the standard deviations on triplicate samples.

2.3.5 Biofilm growth and *S. aureus* viability on Ti discs

The abilities of the PBSe coatings to inhibit *S. aureus* biofilm formation were investigated both with and without IH. *S. aureus* was selected because it is often associated with prosthetic joint infections.⁷¹ Biofilms were grown on PBSe-coated Ti discs in TSB supplemented with 1% glucose for 48 h at 37 °C and then they were quantified by crystal violet staining. The incorporation of 2.5% (w/w) of rifampicin into

the PEA coating without IH reduced biofilm formation to 36% compared to the same PEA coating alone (Figure 2.10A). IH alone, performed at 2 h and 24 h on PBSe-coated Ti discs resulted in a 50% reduction in biofilm formation compared to the control. Thus, neither IH nor antibiotic alone under these conditions was able to sufficiently reduce biofilm formation. However, the use of IH with rifampicin-loaded PBSe coatings resulted in a 96% reduction in biofilm formation compared to the control, showing a potential synergistic effect.

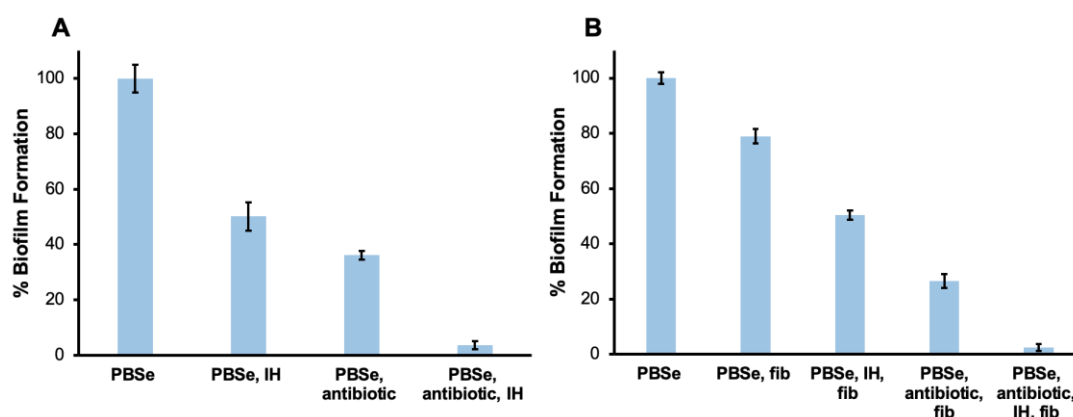


Figure 2.10: Biofilm formation as measured by the crystal violet assay for *S. aureus* seeded on A) PBSe coatings with different combinations of antibiotic and IH; B) combinations of antibiotic and IH following treatment of PBSe coatings with fibrinogen, compared to no fibrinogen treatment. All treatments led to the suppression of biofilm formation, with a combination of antibiotic and IH providing a large, synergistic effect both in the presence and absence of fibrinogen. All samples are normalized to untreated PBSe without IH or antibiotic (100% biofilm). All sample groups were statistically significantly different ($p < 0.05$, $N=3$).

The effect of fibrinogen adsorption on the antibiofilm properties of the coatings and IH treatment was also investigated. Human plasma fibrinogen is a soluble glycoprotein found in high concentrations (2 – 3 mg/mL) in human plasma.⁷² It has been reported in many studies to be among the most relevant proteins that adsorb to the surfaces of medical devices rapidly after implantation and is subsequently involved in the adhesion of cells, including platelets and leukocytes to biomaterial surfaces^{72,73}. Therefore, it was of interest to evaluate whether fibrinogen adsorption onto the PEA coating would impact

the anti-biofilm behavior of the coatings. The coatings were first treated by immersion in a solution of fibrinogen (25 $\mu\text{g}/\text{mL}$), and then biofilm formation was quantified using crystal violet after different treatment combinations involving antibiotic and IH. Adsorption of fibrinogen led to a $\sim 20\%$ reduction in biofilm formation compared to the PBSe surface without fibrinogen (Figure 2.10B). These results are consistent with a previous report, where the treatment of poly(ethylene terephthalate) and polytetrafluoroethylene surfaces with fibrinogen solutions of similar concentrations led to a substantial reduction of surface adhesivity compared to uncoated surfaces or those coated with lower concentrations of fibrinogen.⁷² As for the untreated PBSe coatings, the incorporation of rifampicin or application of IH led to further reductions in biofilm formation by 50% and 74% compared to the control respectively. Furthermore, the combination of fibrinogen, rifampicin, and IH led to a 97% reduction in biofilm formation. Overall, these results indicate that the adsorption of fibrinogen, expected to occur upon implantation of a PBSe coated device *in vivo*, should not adversely affect the coating's anti-biofilm properties, but rather enhance them.

Biofilm studies were also performed using GFP-labeled *S. aureus*. Inverted fluorescence microscopy images showed similar trends to those observed with crystal violet staining. On the PBSe control coating, it was evident that an established mature biofilm had been formed containing many GFP-expressing bacteria (Figure 2.11A). With IH treatment alone, many GFP-expressing bacteria were still observed, indicating that while the treatment was capable of suppressing biofilm formation, many live bacteria remained (Figure 2.11B). In particular, the live *S. aureus* colonies may be closer to the surface of the PEA coating and further from the selectively heated Ti surface. Many GFP-expressing bacteria were also observed on PEA coatings containing rifampicin but without IH treatment, although less than on the control PEA coating (Figure 2.11C). Thus, neither treatment alone was sufficient. However, using a rifampicin-loaded PBSe coating with IH, very few GFP-expressing *S. aureus* colonies were observed (Figure 2.11D). Thus, these results were in agreement with the results of the crystal violet biofilm staining.

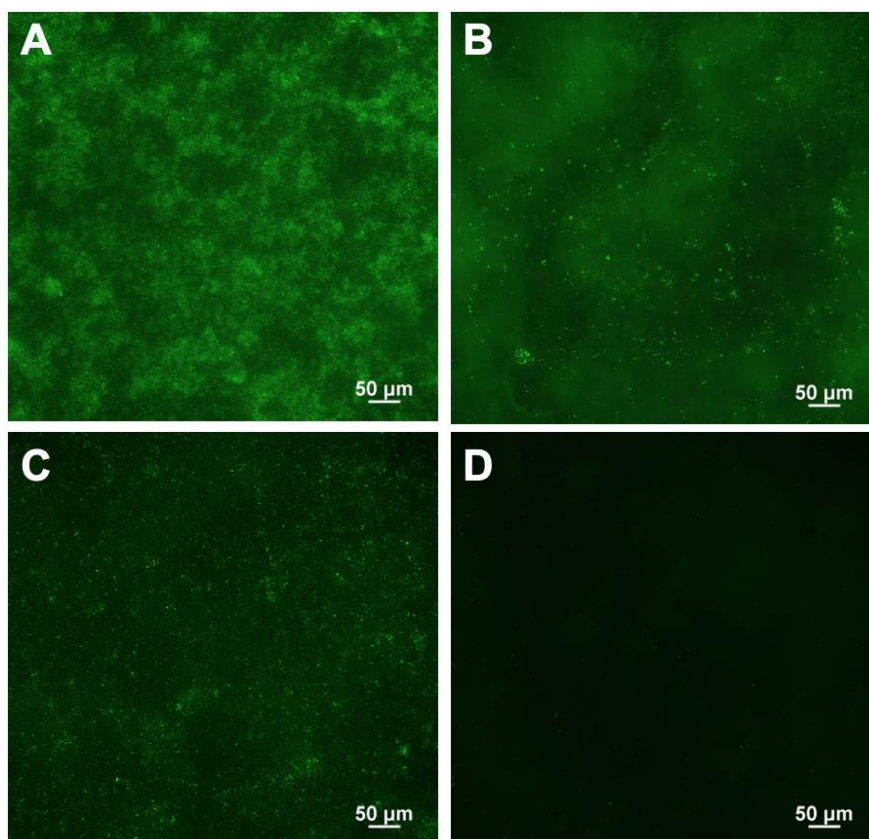


Figure 2.11: Fluorescence microscopy of GFP-expressing *S. aureus* on Ti discs with A) PBSe coating alone; B) PBSe coating with IH treatment at 2 h and 24 h; C) PBSe coating containing 2.5% (w/w) of rifampicin; D) PBSe coating containing 2.5% (w/w) rifampicin and treated with IH at 2 and 24 h. Rifampicin-loaded PBSe coatings treated with IH led to the greatest suppression of GFP-expressing bacteria.

Furthermore, the viability of the bacteria remaining at 48 h after the different treatments was evaluated. The biofilms were disrupted, and the resulting suspensions were plated on agar to quantify the CFUs. The use of IH or antibiotic alone was able to inhibit growth to approximately 95.9 and 96.3% respectively (Table 1). However, PEA coatings with rifampicin in combination with IH resulted in more than a 3-log reduction in *S. aureus* CFUs, showing that the combined treatment was much more effective than either treatment alone. Thus, despite the growth of some biofilm as indicated by the crystal violet staining, at the end of the treatment, a very small fraction of the bacteria remained viable.

Treatment	Inhibition Growth %
PBSe, IH	95.9% \pm 0.3
PBSe, Antibiotic	96.3% \pm 0.1
PBSe, Antibiotic, IH	> 99.9%

Table 1: Quantification of the bacterial biofilm for each treatment in a 48 h biofilm and CFU/mL calculation followed by a percent calculation of inhibited growth.

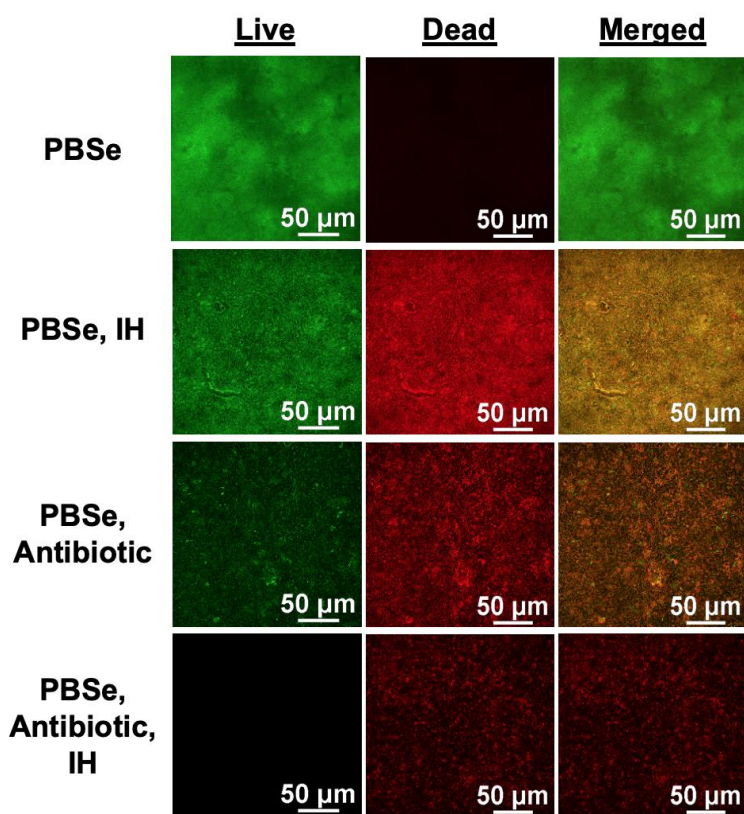


Figure 2.12: Fluorescence microscopy analysis of live and dead *S. aureus* on PBSe coated Ti discs with IH treatment at 2 h and 24 h, PBSe coating containing 2.5% (w/w) of rifampicin, and PBSe coating containing 2.5% (w/w) rifampicin and treated with IH at 2 and 24 h. Rifampicin-loaded PBSe coatings treated with IH led to the lowest population of live bacteria and the highest population of dead bacteria ratio.

To investigate the effectiveness of each treatment concerning the number of live and dead bacteria on the surfaces of each sample, live/dead analyses were performed after 48 h for the different treatments. Many live bacteria were found on the PBSe surface with no treatment (Figure 2.12). On the coating treated with two cycles of intermittent IH (PBSe, IH), substantial numbers of both live and dead bacteria were observed in the biofilm. Fewer live bacteria were observed on the rifampicin-loaded coating without IH (PBSe, Antibiotic). Although these two individual treatments led to similar levels of biofilm quantified by crystal violet, the reduction in live bacteria when the antibiotic was incorporated may result from the killing of bacteria in the later stages of the experiment, after some biofilm had formed. Lastly, the use of a rifampicin-loaded PBSe coating and two cycles of intermittent IH (PBSe, Antibiotic, IH) yielded the fewest live bacteria, along with some dead bacteria on the surface (Figure 2.12).

Overall, these results agree with previous studies where only a combination of heating and solution antibiotic treatment were able to achieve highly effective killing of biofilm bacteria. In our study, a relatively low temperature of 50 °C was used in comparison with other studies investigating the effects of IH alone.^{41,43,46,74} Previous studies using IH alone have found that temperatures between 60 – 90 °C for a duration of 1 – 10 min were required to kill a substantial fraction of biofilm bacteria.^{43,74} Our lower temperature was selected to minimize potential damage to surrounding tissues, but our results are in general agreement with the previous studies, indicating that heating at 50 °C alone is insufficient to prevent biofilm formation. Previous studies have combined IH with antibiotics in solution and showed that IH can increase the sensitivity of biofilm bacteria to antibiotics.⁷⁴ For example, Pijls et al. found that IH at 60 °C provided an increase in the activity of vancomycin, rifampicin, and *N*-acetylcysteine cocktail against *S. aureus* biofilms.⁷⁴ Chopra et al. found that 3 min of IH (reaching ~70 °C) made *P. aeruginosa* biofilms susceptible to otherwise non-inhibitory concentrations of ciprofloxacin.⁴³ The increased susceptibility of bacteria to antibiotics at elevated temperatures is proposed to arise from thermal stimulation of bacterial metabolic activity, which makes the bacteria more sensitive to antibiotics.⁴⁷ However, the preceding studies did not suggest an approach to selectively deliver antibiotics to the bacteria or the biofilm and overcome known challenges such as achieving a sufficient concentration of antibiotic within or near

the biofilm. Our study is the first to use heat to not only kill bacteria directly and increase their susceptibility to antibiotics but also to locally trigger the delivery of antibiotics right at the site of the biofilm.

2.3.6 Mammalian cell viability

It was also important to evaluate the effects of the IH on mammalian cells close to the Ti disc surface. RAW 264.7 macrophages are monocyte/macrophage-like cells originating from the Abelson leukemia virus-transformed cell line derived from BALB/c mice and have been reported as an appropriate model of macrophages.⁷⁵ Macrophages were selected because upon implantation of any biomaterial in the body, they are one of the first groups of cells that interact with the foreign body and play an important role in the immunological response.⁷⁶ It has been shown that following implantation of a material, the standard sequence of immune events includes protein adsorption on the biomaterial surface, macrophage recruitment and adhesion onto the biomaterial surface, followed by the release of chemokines recruiting additional macrophages and other immune cells that help to induce acute inflammation.^{77,78} As a result, it was important to evaluate whether intermittent heating at 50 °C would reduce metabolic activity or kill macrophages seated onto PEA coatings. Several studies have reported that fever temperatures of 38 °C or higher can increase macrophage activity and that macrophage function is responsive to thermal signals, however, temperatures outside the range of a high fever have yet to be clarified.^{79,80} We found that macrophages on the Ti disc exhibited 79% metabolic activity compared to the tissue-cultured well control surface, whereas these cells on PEA coating had 61% metabolic activity (Figure 2.13). After exposure to a 1 h cycle at 50 °C, the metabolic activity of the macrophages is reduced to approximately half (29%) when compared to the PEA coating without IH. These results show that there is a significant reduction in the metabolic activity of macrophages, likely indicating the presence of dead macrophages after the IH cycle. It is important to note that these results are indicative of mammalian cells that are closest or in direct contact with the heated Ti disc via IH, which reaches 50 °C, and the effects on more distant cells, where the temperature is much less elevated (e.g., 40 °C) would be expected to be much less. Furthermore, the presence of remaining metabolically active cells even after the IH treatment suggests the potential for

the cells to regenerate after the treatment. Compared to the thermal energy generated in cortical bone drilling or polymerization of acrylic bone cement, the set temperature we have chosen is reasonably safe.^{45,67,68,70}

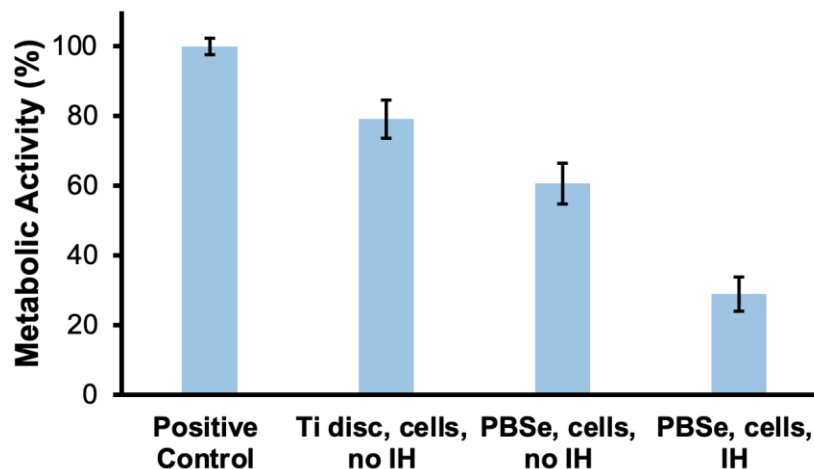


Figure 2.13 The metabolic activity of macrophages was measured using an MTT assay to determine the viability of adhered macrophages on PEA coated and uncoated samples and subjected to one cycle of intermittent IH at 50 °C. All samples are normalized to the positive control, tissue-cultured well surface (100% metabolic activity). All sample groups were statistically significantly different ($p < 0.05$, $N=3$).

2.3.7 Conclusions

PEA coatings containing rifampicin were successfully prepared on 3D-printed Ti discs and exhibited T_g values just above 37 °C. In the absence of direct heating or IH, the PBSe coatings slowly eroded and released rifampicin over 100 days but at temperatures above the PBSe T_g accelerated drug release was observed. Five six-minute cycles of intermittent IH to a maximum of 50 °C over a period of 1 h resulted in 26% release, while the surrounding medium did not exceed 40 °C. Both heating and rifampicin individually reduced *S. aureus* biofilm formation but the use of rifampicin-loaded PEA coatings in combination with two 1 h IH treatments over a 48 h period reduced biofilm formation by 96%, showing a potential synergistic effect. The anti-biofilm properties were maintained even with the adsorption of fibrinogen to the surface of PEA coatings. In addition, >99.9% of the bacteria on the surface was killed during the 48 h treatment. These results

demonstrate a novel PEA-based implant coating as an antibiotic carrier with externally triggerable antibiotic release to ODRI. Future work will involve further studies of the antibacterial properties of these coatings, their compatibility with mammalian cells, and their *in vivo* behavior.

2.4 References

1. Bozic, K. J. *et al.* The epidemiology of revision total knee arthroplasty in the United States. *Clin Orthop Relat Res* **468**, 45–51 (2010).
2. Hernández-Vaquero, D. *et al.* Treatment of periprosthetic infections: an economic analysis. *ScientificWorldJournal* **2013**, (2013).
3. Kamath, A. F. *et al.* Quantifying the Burden of Revision Total Joint Arthroplasty for Periprosthetic Infection. *J Arthroplasty* **30**, 1492–1497 (2015).
4. Ellis, S. & Ong, E. Disseminated Infections: A Clinical Overview. *Molecular Medical Microbiology* 637 (2015) doi:10.1016/B978-0-12-397169-2.00036-6.
5. Moriarty, T. F. *et al.* Orthopaedic device-related infection: current and future interventions for improved prevention and treatment. *EFORT Open Rev* **1**, 89–99 (2017).
6. Kim, H. S. *et al.* Current and Future Burden of Periprosthetic Joint Infection from National Claim Database. *J Korean Med Sci* **35**, (2020).
7. Bhandari, M., Smith, J., Miller, L. E. & Block, J. E. Clinical and economic burden of revision knee arthroplasty. *Clin Med Insights Arthritis Musculoskelet Disord* **5**, 89–94 (2012).
8. Premkumar, A. *et al.* Projected Economic Burden of Periprosthetic Joint Infection of the Hip and Knee in the United States. *J Arthroplasty* **36**, 1484-1489.e3 (2021).
9. Vigeant, M. A. S., Ford, R. M., Wagner, M. & Tamm, L. K. Reversible and irreversible adhesion of motile *Escherichia coli* cells analyzed by total internal reflection aqueous fluorescence microscopy. *Appl Environ Microbiol* **68**, 2794–2801 (2002).
10. Schuster, J. J. & Marx, G. H. Biofilm architecture. *Advances in Biochemical Engineering/biotechnology* **146**, 77–96 (2014).
11. Srivastav, A. K., Nadkarni, B., Srivastav, S., Mittal, V. & Agarwal, S. Prophylactic use of antibiotic-loaded bone cement in primary total knee arthroplasty: Justified or not? *Indian Journal of Orthopaedics* **43**, 259 (2009).

12. Boddapati, V. *et al.* Revision Total Knee Arthroplasty for Periprosthetic Joint Infection Is Associated With Increased Postoperative Morbidity and Mortality Relative to Noninfectious Revisions. *J Arthroplasty* **33**, 521–526 (2018).
13. Mirza, Y. H., Tansey, R., Sukeik, M., Shaath, M. & Haddad, F. S. Suppl-2, M6: Biofilm and the Role of Antibiotics in the Treatment of Periprosthetic Hip and Knee Joint Infections. *The Open Orthopaedics Journal* **10**, 636 (2016).
14. Sharma, D., Misba, L. & Khan, A. U. Antibiotics versus biofilm: an emerging battleground in microbial communities. *Antimicrobial Resistance & Infection Control* **2019** 8:1 **8**, 1–10 (2019).
15. Darouiche, R. O. Treatment of infections associated with surgical implants. *N Engl J Med* **350**, 1422–1429 (2004).
16. Charette, R. S. & Melnic, C. M. Two-Stage Revision Arthroplasty for the Treatment of Prosthetic Joint Infection. *Curr Rev Musculoskelet Med* **11**, 332–340 (2018).
17. Slane, J., Gietman, B. & Squire, M. Antibiotic elution from acrylic bone cement loaded with high doses of tobramycin and vancomycin. *J Orthop Res* **36**, 1078–1085 (2018).
18. Hinarejos, P. *et al.* Use of antibiotic-loaded cement in total knee arthroplasty. *World Journal of Orthopedics* **6**, 877 (2015).
19. Laycock, P. A. *et al.* In Vitro Efficacy of Antibiotics Released from Calcium Sulfate Bone Void Filler Beads. *Materials (Basel)* **11**, (2018).
20. Anagnostakos, K., Hitzler, P., Pape, D., Kohn, D. & Kelm, J. Persistence of bacterial growth on antibiotic-loaded beads: is it actually a problem? *Acta Orthop* **79**, 302–307 (2008).
21. Alt, V. Antimicrobial coated implants in trauma and orthopaedics-A clinical review and risk-benefit analysis. *Injury* **48**, 599–607 (2017).
22. Metsemakers, W. J., Moriarty, T. F., Nijs, S., Pape, H. C. & Richards, R. G. Influence of implant properties and local delivery systems on the outcome in operative fracture care. *Injury* **47**, 595–604 (2016).
23. Funk, G. A., Burkes, J. C., Cole, K. A., Rahaman, M. N. & Mciff, T. E. Antibiotic Elution and Mechanical Strength of PMMA Bone Cement Loaded With Borate Bioactive Glass. *Journal of Bone and Joint Infection* **3**, 187 (2018).
24. McConoughey, S. J., Howlin, R. P., Wiseman, J., Stoodley, P. & Calhoun, J. H. Comparing PMMA and calcium sulfate as carriers for the local delivery of antibiotics to infected surgical sites. *J Biomed Mater Res B Appl Biomater* **103**, 870–877 (2015).

25. Dusane, D. H. *et al.* Effects of loading concentration, blood and synovial fluid on antibiotic release and anti-biofilm activity of bone cement beads. *J Control Release* **248**, 24–32 (2017).
26. Roberts, R., McConoughey, S. J. & Calhoun, J. H. Size and composition of synthetic calcium sulfate beads influence dissolution and elution rates in vitro. *J Biomed Mater Res B Appl Biomater* **102**, 667–673 (2014).
27. Aiken, S. S., Cooper, J. J., Florance, H., Robinson, M. T. & Michell, S. Local release of antibiotics for surgical site infection management using high-purity calcium sulfate: an in vitro elution study. *Surg Infect (Larchmt)* **16**, 54–61 (2015).
28. Cloutier, M., Mantovani, D. & Rosei, F. Antibacterial Coatings: Challenges, Perspectives, and Opportunities. *Trends Biotechnol* **33**, 637–652 (2015).
29. Yilmaz Atay, H. Antibacterial Activity of Chitosan-Based Systems. *Functional Chitosan* 457 (2020) doi:10.1007/978-981-15-0263-7_15.
30. Teixeira-Santos, R., Lima, M., Gomes, L. C. & Mergulhão, F. J. Antimicrobial coatings based on chitosan to prevent implant-associated infections: A systematic review. *iScience* **24**, 103480 (2021).
31. Jiao, Y. *et al.* Quaternary ammonium-based biomedical materials: State-of-the-art, toxicological aspects and antimicrobial resistance. *Progress in Polymer Science* **71**, 53 (2017).
32. Jennings, M. C., Minbiole, K. P. C. & Wuest, W. M. Quaternary Ammonium Compounds: An Antimicrobial Mainstay and Platform for Innovation to Address Bacterial Resistance. *ACS Infectious Diseases* **1**, 288–303 (2016).
33. Vela-Cano, M., Garcia-Fontana, C., Osorio, F., González-Martinez, A. & González-López, J. Silver-Derived Antimicrobial Coatings for the Prevention of Microbial Biofilms in Metal Pipes. *Water, Air, and Soil Pollution* **232**, 1–11 (2021).
34. Sim, W., Barnard, R. T., Blaskovich, M. A. T. & Ziora, Z. M. Antimicrobial Silver in Medicinal and Consumer Applications: A Patent Review of the Past Decade (2007–2017). *Antibiotics* **7**, (2018).
35. Park, H. J. *et al.* Silver-ion-mediated reactive oxygen species generation affecting bactericidal activity. *Water Res* **43**, 1027–1032 (2009).
36. Fabritius, M. *et al.* Antimicrobial Silver Multilayer Coating for Prevention of Bacterial Colonization of Orthopedic Implants. *Materials* **13**, (2020).
37. Brennan, S. A. *et al.* Instructional review: General orthopaedics silver nanoparticles and their orthopaedic applications. *Bone and Joint Journal* **97-B**, 582–589 (2015).

38. You, J., Zhang, Y. & Hu, Z. Bacteria and bacteriophage inactivation by silver and zinc oxide nanoparticles. *Colloids Surf B Biointerfaces* **85**, 161–167 (2011).
39. Campoccia, D., Montanaro, L., Speziale, P. & Arciola, C. R. Antibiotic-loaded biomaterials and the risks for the spread of antibiotic resistance following their prophylactic and therapeutic clinical use. *Biomaterials* **31**, 6363–6377 (2010).
40. Liu, X. *et al.* Comprehensive understanding of magnetic hyperthermia for improving antitumor therapeutic efficacy. *Theranostics* **10**, 3793 (2020).
41. Pijls, B. G., Sanders, I. M. J. G., Kuijper, E. J. & Nelissen, R. G. H. H. Non-contact electromagnetic induction heating for eradicating bacteria and yeasts on biomaterials and possible relevance to orthopaedic implant infections: In vitro findings. *Bone Joint Res* **6**, 323–330 (2017).
42. Pijls, B. G., Sanders, I. M. J. G., Kuijper, E. J. & Nelissen, R. G. H. H. Segmental induction heating of orthopaedic metal implants. *Bone Joint Res* **7**, 609–619 (2018).
43. Chopra, R. *et al.* Employing high-frequency alternating magnetic fields for the non-invasive treatment of prosthetic joint infections. *Sci Rep* **7**, (2017).
44. Kurose, H., Miyagi, D., Takahashi, N., Uchida, N. & Kawanaka, K. 3-D Eddy current analysis of induction heating apparatus considering heat emission, heat conduction, and temperature dependence of magnetic characteristics. *IEEE Transactions on Magnetics* **45**, 1847–1850 (2009).
45. Müller, C. W. *et al.* Transcutaneous electromagnetic induction heating of an intramedullary nickel-titanium shape memory implant. *Int Orthop* **38**, 2551–2557 (2014).
46. Pijls, B. G., Sanders, I. M. J. G., Kuijper, E. J. & Nelissen, R. G. H. H. Induction heating for eradicating *Staphylococcus epidermidis* from biofilm. *Bone & Joint Research* **9**, 192 (2020).
47. Ricker, E. B. & Nuxoll, E. Synergistic effects of heat and antibiotics on *Pseudomonas aeruginosa* biofilms. *Biofouling* **33**, 855–866 (2017).
48. Hajdu, S. *et al.* Increased Temperature Enhances the Antimicrobial Effects of Daptomycin, Vancomycin, Tigecycline, Fosfomicin, and Cefamandole on Staphylococcal Biofilms. *Antimicrobial Agents and Chemotherapy* **54**, 4078 (2010).
49. Rodriguez-Galan, A., Franco, L. & Puiggali, J. Degradable Poly(ester amide)s for Biomedical Applications. *Polymers 2011, Vol. 3, Pages 65-99* **3**, 65–99 (2010).
50. Winnacker, M. & Rieger, B. Poly(ester amide)s: recent insights into synthesis, stability and biomedical applications. *Polymer Chemistry* **7**, 7039–7046 (2016).

51. Soleimani, A., Drappel, S., Carlini, R., Goredema, A. & Gillies, E. R. Structure-property relationships for a series of poly(ester amide)s containing amino acids. *Industrial and Engineering Chemistry Research* **53**, 1452–1460 (2014).
52. Villamagna, I. J., Gordon, T. N., Hurtig, M. B., Beier, F. & Gillies, E. R. Poly(ester amide) particles for controlled delivery of celecoxib. *J Biomed Mater Res A* **107**, 1235–1243 (2019).
53. Peters, T. *et al.* Evaluation of poly(esteramide) (PEA) and polyester (PLGA) microspheres as intravitreal drug delivery systems in albino rats. *Biomaterials* **124**, 157–168 (2017).
54. Zhang, S. *et al.* Poly(ester amide)-based hybrid hydrogels for efficient transdermal insulin delivery. *Journal of Materials Chemistry B* **6**, 6723–6730 (2018).
55. Knight, D. K., Gillies, E. R. & Mequanint, K. Strategies in functional poly(ester amide) syntheses to study human coronary artery smooth muscle cell interactions. *Biomacromolecules* **12**, 2475–2487 (2011).
56. Ghosal, K., Latha, M. S. & Thomas, S. Poly(ester amides) (PEAs) – Scaffold for tissue engineering applications. *European Polymer Journal* **60**, 58–68 (2014).
57. Lips, P. A. M. *et al.* Biocompatibility and degradation of aliphatic segmented poly(ester amide)s: in vitro and in vivo evaluation. *J Biomed Mater Res A* **76**, 699–710 (2006).
58. Kropp, M. *et al.* Biocompatibility of Poly(ester amide) (PEA) Microfibrils in Ocular Tissues. *Polymers 2014, Vol. 6, Pages 243-260* **6**, 243–260 (2014).
59. Grossman, A. B., Burgin, D. J. & Rice, K. C. Quantification of *Staphylococcus aureus* Biofilm Formation by Crystal Violet and Confocal Microscopy. *Methods Mol Biol* **2341**, 69–78 (2021).
60. Lee, J. S., Bae, Y. M., Lee, S. Y. & Lee, S. Y. Biofilm Formation of *Staphylococcus aureus* on Various Surfaces and Their Resistance to Chlorine Sanitizer. *J Food Sci* **80**, M2279–M2286 (2015).
61. Gries, C. M. *et al.* Potassium Uptake Modulates *Staphylococcus aureus* Metabolism. *mSphere* **1**, (2016).
62. Flannagan, R. S. & Heinrichs, D. E. A fluorescence based-proliferation assay for the identification of replicating bacteria within host cells. *Frontiers in Microbiology* **9**, 3084 (2018).
63. Alves, R. *et al.* Thermal behavior and decomposition kinetics of rifampicin polymorphs under isothermal and non-isothermal conditions. *Brazilian Journal of Pharmaceutical Sciences* **46**, 343–351 (2010).

64. Halal, S., Roemer, R. B., Oleson, J. R. & Cetas, T. C. Magnetic induction heating of tissue: numerical evaluation of tumor temperature distributions. *Int J Radiat Oncol Biol Phys* **9**, 881–891 (1983).
65. van Rhoon, G. C. *et al.* CEM43°C thermal dose thresholds: a potential guide for magnetic resonance radiofrequency exposure levels? *Eur Radiol* **23**, 2215 (2013).
66. Dewhurst, M. W., Viglianti, B. L., Lora-Michiels, M., Hanson, M. & Hoopes, P. J. Basic principles of thermal dosimetry and thermal thresholds for tissue damage from hyperthermia. *Int J Hyperthermia* **19**, 267–294 (2003).
67. Timon, C. & Keady, C. Thermal Osteonecrosis Caused by Bone Drilling in Orthopedic Surgery: A Literature Review. *Cureus* **11**, (2019).
68. Deramond, H., Wright, N. T. & Belkoff, S. M. Temperature elevation caused by bone cement polymerization during vertebroplasty. *Bone* **25**, (1999).
69. Samara, E. *et al.* Antibiotic stability over six weeks in aqueous solution at body temperature with and without heat treatment that mimics the curing of bone cement. *Bone Joint Res* **6**, 296–306 (2017).
70. Fang, C. H. *et al.* Magnetic hyperthermia enhance the treatment efficacy of peri-implant osteomyelitis. *BMC Infect Dis* **17**, (2017).
71. Baratz, M. D., Hallmark, R., Odum, S. M. & Springer, B. D. Twenty Percent of Patients May Remain Colonized With Methicillin-resistant Staphylococcus aureus Despite a Decolonization Protocol in Patients Undergoing Elective Total Joint Arthroplasty. *Clin Orthop Relat Res* **473**, 2283–2290 (2015).
72. Safiullin, R. *et al.* Fibrinogen matrix deposited on the surface of biomaterials acts as a natural anti-adhesive coating. *Biomaterials* **67**, 151–159 (2015).
73. Horbett, T. A. Fibrinogen adsorption to biomaterials. *Journal of Biomedical Materials Research Part A* **106**, 2777–2788 (2018).
74. Pijls, B. G., Sanders, I. M. J. G., Kuijper, E. J. & Nelissen, R. G. H. H. Synergy between induction heating, antibiotics, and N-acetylcysteine eradicates Staphylococcus aureus from biofilm. *Int J Hyperthermia* **37**, 130–136 (2020).
75. Taciak, B. *et al.* Evaluation of phenotypic and functional stability of RAW 264.7 cell line through serial passages. *PLoS ONE* **13**, (2018).
76. Balabiyev, A. *et al.* Fibrin polymer on the surface of biomaterial implants drives the foreign body reaction. *Biomaterials* **277**, (2021).
77. Kzhyshkowska, J. *et al.* Macrophage responses to implants: prospects for personalized medicine. *Journal of Leukocyte Biology* **98**, 953–962 (2015).

78. Anderson, J. M., Rodriguez, A. & Chang, D. T. FOREIGN BODY REACTION TO BIOMATERIALS. *Semin Immunol* **20**, 86 (2008).
79. Evans, S. S., Repasky, E. A. & Fisher, D. T. Fever and the thermal regulation of immunity: the immune system feels the heat. *Nat Rev Immunol* **15**, 335 (2015).
80. Lee, C. T., Zhong, L., Mace, T. A. & Repasky, E. A. Elevation in Body Temperature to Fever Range Enhances and Prolongs Subsequent Responsiveness of Macrophages to Endotoxin Challenge. *PLoS ONE* **7**, (2012).

Chapter 3

3 Summary and future work

This thesis addresses unmet needs related to treating and preventing ODRI with the proposal of an antibiotic-loaded PEA-based coating that can be triggered externally and on-demand via an alternating electromagnetic field using IH.

In Chapter 2, the synthesis and characterization of the polymer PBSe was described, demonstrating the successful preparation of a PEA with a T_g of 39°C, just above a physiological temperature. PBSe was co-dissolved with rifampicin at varying weight percentages in the range of 2.5 – 10%, resulting in T_g values of 41 – 45 °C. In the absence of heating, rifampicin-loaded PBSe coatings eroded and released the drug very slowly, with 17% released over 100 days for the 2.5% coating. On the other hand, incubation of these coatings at higher temperatures above the T_g of PBSe resulted in an accelerated release of rifampicin with little to no degradation of the polymer. The IH process was optimized to enable five 6 min heating cycles with a maximum temperature of 50 °C to be performed over 1 h without the surrounding bath temperature exceeding 40 °C. Rifampicin release was accelerated under these conditions with 26% of the drug released over the 1 h treatment. Crystal violet staining and fluorescence microscopy of *S. aureus* biofilms on PBSe-coated titanium discs indicated that the use of antibiotic or IH individually can reduce biofilm formation to 36%, and 50%, respectively. However, the use of intermittent IH and rifampicin-loaded PBSe coatings resulted in less than 5% biofilm formation compared to the control, showing a potential synergistic effect. This effect still held after the adsorption of fibrinogen onto PBSe-coatings. Furthermore, the bacteria viability post 48 h for all treatments was found to show that the use of IH or antibiotic alone inhibited growth to approximately 96 and 97% respectively. However, the combination of a rifampicin-loaded PBSe coating and intermittent IH resulted in a 3-log reduction of 99.98% in *S. aureus* CFUs. These conditions were also tested against macrophages using an MTT assay. The data demonstrated adherence and normal metabolic activity of macrophages on PBSe-coated and uncoated Ti discs. When PBSe coatings were subjected to the 1 h protocol (max 50 °C), the metabolic activity of

macrophages was reduced to 29% compared to the same coating in the absence of IH demonstrating the potential feasibility of using these conditions *in vivo*.

While this novel thermo-responsive antibiotic-eluting PEA coating is promising and shows great potential in the orthopedic field, further research is still needed. The next steps will be to evaluate antibiotic-loaded PEA coatings *in vivo* both in the absence and presence of IH and investigate whether the approach can treat or prevent ODRI. Pre-clinical studies generally involve the use of small animal models, such as mice or rats, and will be a good starting point to determine if the coating is well-tolerating and if adjustments to the IH protocol are required. For example, changes that could be explored include the use of shorter intervals but with more power resulting in a higher set temperature, longer breaks in between IH, or several cycles of IH compared to the two cycles of IH in a 48 h period that was used in most of the studies described in Chapter 2. Although we can effectively heat the surface of a Ti disc using our IH protocol and device, an improved protocol and design of the IH device will be needed to safely accommodate a small animal model.

The decision to employ a drop-casting method was taken so that the exact amount of drug released from PEA coatings could be calculated. In future studies using hip, knee, or shoulder implants it may be necessary to use an alternative coating method that is more efficient in creating a uniform layer for complex shapes. One method that was not mentioned in this study but that I tested was spray coating. Rifampicin-PEA coatings could be co-dissolved using dichloromethane, an organic solvent that readily evaporates at room temperature. Using a thin layer chromatography reagent sprayer connected to an air pump and a 250 mL round bottom flask with 10 mL of a stock solution of rifampicin-PEA a uniform coating could be achieved on the Ti discs. This spray-coating method can also be employed in future studies to spray complex hip or knee implant shapes. Dip coating would be another possibility.

The mechanical properties of the antibiotic-loaded PEA coating should also be explored in a future study. Examination of how well the PEA coating adheres to the surfaces of different biomaterials such as chromium cobalt or stainless may also prove useful. There

have been numerous studies detailing the use of PEAs as hydrogels and other implanted materials such as particles, but for the purpose of coating an orthopedic device, the mechanical properties should still be investigated.¹⁻⁴ Examining its Young's modulus, tensile and compressive strength along with how the coating is affected during mechanical movement of a hip and knee implant may also help provide insight on how well the coating adheres over the long-term. Additionally, upon implantation of PEA-coated orthopedic devices, it will be important to evaluate how the coating will influence bone cell adherence and if there are any limitations involved with the fixation of the orthopedic devices and bone growth surrounding the device.

The design of the PEA coating had also taken into consideration antibiotic-resistant bacteria as part of one of the main problems of ODRI. The main issue that has been reported in many studies is the continued and regular use of antibiotics such as vancomycin and gentamicin combined with the same antibiotic carriers (PMMA bone cement and calcium sulfate).⁵⁻¹² The repeated use of these antibiotics can induce resistant bacteria and ultimately exacerbate infection rates in the orthopedic field.¹³⁻¹⁵ Many studies have begun combining various antibiotics to combat antibiotic-resistant bacteria.^{16,17} In addition to the work described in Chapter 2, I performed preliminary studies to investigate using a combination of vancomycin and rifampicin in PEA coatings to combat this problem. I found that although I was able to successfully use both antibiotics within the PEA coatings and achieve rapid release at high temperatures, the T_g was reduced below physiological temperature. This may or may not be a problem, and polymers generally undergo a gradual reduction in viscosity around the T_g . At higher temperatures, there was an initial burst release of vancomycin as it readily dissolved in PBS, followed by a slower release of rifampicin from PEA coatings. It may be necessary to tweak the thermal properties of PBSe to achieve a higher T_g . This can be done by incorporating different monomers with more rigid structures.

3.1 References

1. Bozic, K. J. *et al.* The epidemiology of revision total knee arthroplasty in the United States. *Clin Orthop Relat Res* **468**, 45–51 (2010).
1. Zhang, S. *et al.* Poly(ester amide)-based hybrid hydrogels for efficient transdermal insulin delivery. *Journal of Materials Chemistry B* **6**, 6723–6730 (2018).
2. Ghosal, K., Latha, M. S. & Thomas, S. Poly(ester amides) (PEAs) – Scaffold for tissue engineering applications. *European Polymer Journal* **60**, 58–68 (2014).
3. Winnacker, M. & Rieger, B. Poly(ester amide)s: recent insights into synthesis, stability and biomedical applications. *Polymer Chemistry* **7**, 7039–7046 (2016).
4. Soleimani, A., Drappel, S., Carlini, R., Goredema, A. & Gillies, E. R. Structure-property relationships for a series of poly(ester amide)s containing amino acids. *Industrial and Engineering Chemistry Research* **53**, 1452–1460 (2014).
5. Zhang, H. *et al.* Vancomycin-loaded titanium coatings with an interconnected micro-patterned structure for prophylaxis of infections: an in vivo study. *RSC Advances* **8**, 9223–9231 (2018).
6. Boelch, S. P. *et al.* Comparison of Elution Characteristics and Compressive Strength of Biantibiotic-Loaded PMMA Bone Cement for Spacers: Copal® Spacem with Gentamicin and Vancomycin versus Palacos® R+G with Vancomycin. *Biomed Res Int* **2018**, (2018).
7. Bishop, A. R., Kim, S., Squire, M. W., Rose, W. E. & Ploeg, H. L. Vancomycin elution, activity and impact on mechanical properties when added to orthopedic bone cement. *J Mech Behav Biomed Mater* **87**, 80–86 (2018).
8. Slane, J., Gietman, B. & Squire, M. Antibiotic elution from acrylic bone cement loaded with high doses of tobramycin and vancomycin. *J Orthop Res* **36**, 1078–1085 (2018).
9. Long, P. H. Medical Devices in Orthopedic Applications. *Toxicologic Pathology* **36**, 85–91 (2008).
10. Bistolfi, A. *et al.* Antibiotic-Loaded Cement in Orthopedic Surgery: A Review. *ISRN Orthopedics* **2011**, 1–8 (2011).
11. Hinarejos, P. *et al.* Use of antibiotic-loaded cement in total knee arthroplasty. *World Journal of Orthopedics* **6**, 877 (2015).
12. Gasparini, G. *et al.* Drug elution from high-dose antibiotic-loaded acrylic cement: a comparative, in vitro study. *Orthopedics* **37**, e999–e1005 (2014).

13. Delcour, A. H. Outer Membrane Permeability and Antibiotic Resistance. *Biochim Biophys Acta* **1794**, 808 (2009).
14. Sharma, D., Misba, L. & Khan, A. U. Antibiotics versus biofilm: an emerging battleground in microbial communities. *Antimicrobial Resistance & Infection Control* **2019** 8:1 **8**, 1–10 (2019).
15. Campoccia, D., Montanaro, L., Speziale, P. & Arciola, C. R. Antibiotic-loaded biomaterials and the risks for the spread of antibiotic resistance following their prophylactic and therapeutic clinical use. *Biomaterials* **31**, 6363–6377 (2010).
16. Ricker, E. B. & Nuxoll, E. Synergistic effects of heat and antibiotics on *Pseudomonas aeruginosa* biofilms. *Biofouling* **33**, 855–866 (2017).
17. Pijls, B. G., Sanders, I. M. J. G., Kuijper, E. J. & Nelissen, R. G. H. H. Synergy between induction heating, antibiotics, and N-acetylcysteine eradicates *Staphylococcus aureus* from biofilm. *Int J Hyperthermia* **37**, 130–136 (2020).

Appendices

Appendix 1 – Supporting information for Chapter 2: Thermo-responsive Antibiotic-Eluting Coatings for Treating Infection near Orthopedic Implants

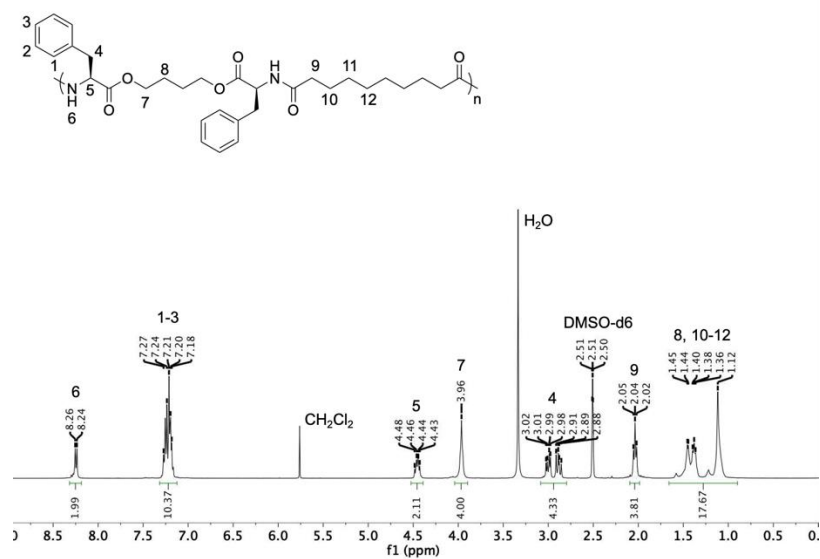


Figure A1. $^1\text{H-NMR}$ spectrum of PBSe (DMSO- d_6 , 400 MHz).

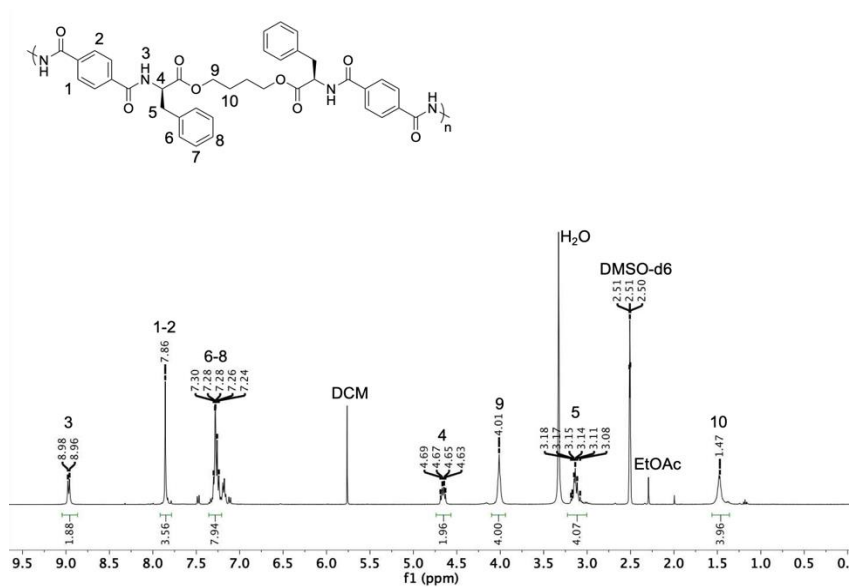


Figure A2. $^1\text{H-NMR}$ spectrum of PBTe (DMSO- d_6 , 400 MHz).

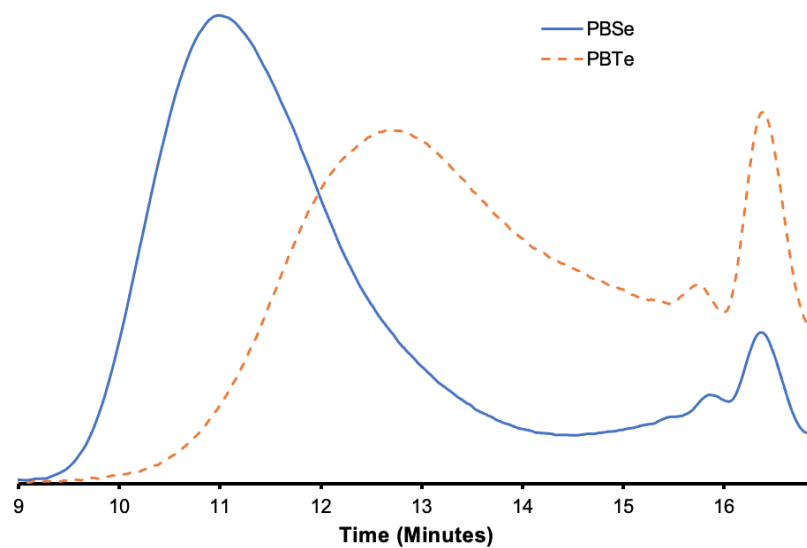


Figure A3. Overlay of SEC traces for PBSe and control PBTe

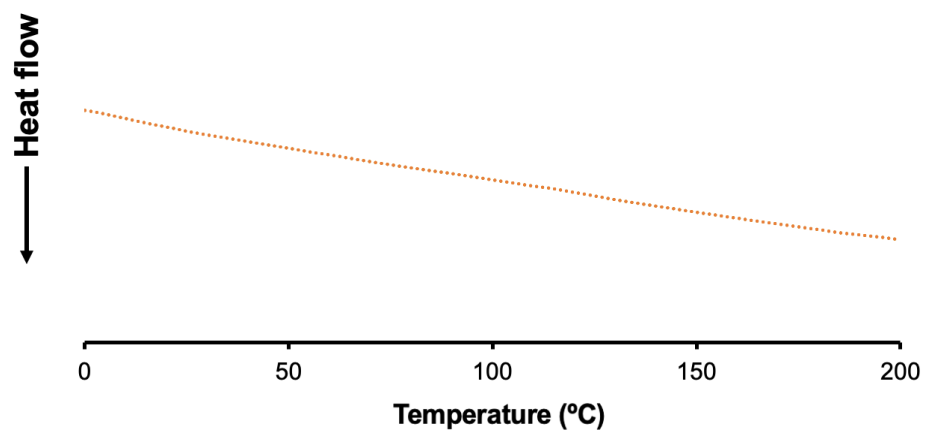


Figure A4. DSC thermograph of rifampicin

Appendix 2 – Permission to reuse copyrighted material

Order History

Order history results only apply to orders placed on copyright.com. You can view and search your orders placed on Marketplace within the [View](#) and [Pay Invoices](#) tab within Manage Account.

View Orders	View Order Details	View RIGHTSLINK Orders
View: Completed Pending Canceled Credited Denied Sort orders by: Order Date <input type="checkbox"/> Ascending <input checked="" type="radio"/> Descending		
LICENSE #: 5343230456009 Order Date: 07/06/2022 View printable order	Biomaterials Title: Staphylococcus aureus adhesion to titanium oxide surfaces coated with non-functionalized and peptide-functionalized poly(L-lysine)-grafted-poly(ethylene glycol) copolymers Type of use: reuse in a thesis/dissertation	Fee: 0.00 USD
LICENSE #: 5342670043531 Order Date: 07/05/2022 View printable order	Pharmacotherapy, The Journal of Human Pharmacology and Drug Therapy Title: Trowels and Tribulations: Review of Antimicrobial-Impregnated Bone Cements in Prosthetic Joint Surgery Type of use: Dissertation/Thesis	Fee: 0.00 USD
LICENSE #: 5342100091828 Order Date: 07/04/2022 View printable order	Macromolecular Bioscience Title: Smart Titanium Coating Composed of Antibiotic Conjugated Peptides as an Infection-Responsive Antibacterial Agent Type of use: Dissertation/Thesis	Fee: 0.00 USD
LICENSE #: 5342091354590 Order Date: 07/04/2022 View printable order	Journal of Controlled Release Title: pH-controlled delivery of gentamicin sulfate from orthopedic devices preventing nosocomial infections Type of use: reuse in a thesis/dissertation	Fee: 0.00 USD

Order Details

1. New journal of chemistry

Article: Doxorubicin release by magnetic inductive heating and in vivo hyperthermia-chemotherapy combined c...

Billing Status:
Open

[Print License](#)

Order License ID	1245799-1	Type of use	Republish in a thesis/dissert...
Order detail status	Completed	Publisher	ROYAL SOCIETY OF CHEMIST...
ISSN	1369-9261	Portion	Image/photo/illustration
			0.00 USD

From: amarendra roy [REDACTED]
Date: Monday, July 4, 2022 at 3:47 PM
To: Jan Kwan [REDACTED]
Subject: Re: Permission to use figure from research article for Master thesis

Great. You can use that and must keep contact with me for further development.

Curriculum Vitae

Name: Jan C. Kwan

Post-secondary Education and Degrees: University of Western Ontario
London, Ontario, Canada
2020-2022, M.E.Sc.

Queen's University
Kingston, Ontario, Canada
2015-2019, B.Sc.

Honours and Awards: 2nd Place Oral Presentation Prize
37th Annual Meeting of the Canadian Biomaterials Society 2022
“Thermo-Responsive Coatings for Treating Infection near Orthopedic Implants”

Top Master Student Award
5th Biennial Canadian Bone and Joint 2022 Conference
“Thermo-Responsive Coatings for Treating Infection near Orthopedic Implants”

Conference Presentations 5th Biennial Canadian Bone and Joint 2022 Conference
(Oral Presentation)

37th Annual Meeting of the Canadian Biomaterials Society 2022 (Oral Presentation)

Center for Advanced Materials and Biomaterials 2021
(ePoster session)

London Health Research Day 2021
(ePoster session)

Related Work Experience Graduate Research Assistant
The University of Western Ontario
2020-2022

Graduate Teaching Assistant
The University of Western Ontario
2021-2022

Summer Research Assistant
Biomedical Implant Technology Inc.
2015-2020